AFRL-HE-BR-TR-2007-0050

Experimental Characterization of Near-Infrared Laser Energy Absorption, Scattering, and Transmittance in Biological Tissue

John Laffitte
David Roelant

Florida International University
Applied Research Center

Michael L. Denton

Northrop Grumman
Information Technology

Robert J. Thomas

Air Force Research Laboratory

March 2007
Interim Report for February 2004 – March 2007

Air Force Research Laboratory
Human Effectiveness Directorate
Directed Energy Bioeffects Division
Optical Radiation Branch
Brooks City-Base, TX 78235

NOTICE AND SIGNATURE PAGE

Using Government drawings, specifications, or other data included in this document for any purpose other than Government procurement does not in any way obligate the U.S. Government. The fact that the Government formulated or supplied the drawings, specifications, or other data does not license the holder or any other person or corporation; or convey any rights or permission to manufacture, use, or sell any patented invention that may relate to them.

This report was cleared for public release by the Air Force Research Laboratory, Brooks City-Base, Public Affairs Office and is available to the general public, including foreign nationals. Copies may be obtained from the Defense Technical Information Center (DTIC) (http://www.dtic.mil).

AFRL-HE-BR-TR-2007-0050 HAS BEEN REVIEWED AND IS APPROVED FOR PUBLICATION IN ACCORDANCE WITH ASSIGNED DISTRIBUTION STATEMENT.

//SIGNED//
ALAN J. RICE, 1Lt, USAF
Contract Monitor

//SIGNED//
GARRETT D. POLHAMUS, Ph.D.
Chief, Directed Energy Bioeffects Division

This report is published in the interest of scientific and technical information exchange, and its publication does not constitute the Government's approval or disapproval of its ideas or findings.

Distribution A – Approved for public release; distribution unlimited

REPORT DOCUMENTATION PAGE

Form Approved
OMB No. 0704-0188

1. REPORT DATE *(DD-MM-YYYY)*	2. REPORT TYPE	3. DATES COVERED *(From - To)*
March 2007	Interim Technical Report	February 2004-March 2007

4. TITLE AND SUBTITLE

Experimental Characterization of Near-Infrared Laser Energy Absorption, Scattering, and Transmittance in Biological Tissue

5a. CONTRACT NUMBER
F41624-02-D-7003

5b. GRANT NUMBER

5c. PROGRAM ELEMENT NUMBER
61102F

6. AUTHOR(S)
[△]John Laffitte, Ph.D., P.E.; [△]David Roelant, Ph.D.; [□]Michael L. Denton, [◊]Robert J. Thomas

5d. PROJECT NUMBER
2312

5e. TASK NUMBER
AH

5f. WORK UNIT NUMBER
02

7. PERFORMING ORGANIZATION NAME(S) AND ADDRESS(ES)

[◊]Air Force Research Laboratory
Human Effectiveness Directorate
Directed Energy Bioeffects Division
Optical Radiation Branch
2624 Louis Bauer Dr.
Brooks City-Base, TX 78235-5128

[□]Northrop Grumman Corporation
Information Technology
4241 Woodcock Drive, Ste B-100
San Antonio, TX 78228-1330

[△]Florida International University
Applied Research Center
10555 West Flagler St, EC 2100
Miami, FL 33174

8. PERFORMING ORGANIZATION REPORT NUMBER
AFRL/HEDO

9. SPONSORING / MONITORING AGENCY NAME(S) AND ADDRESS(ES)
Air Force Materiel Command
Air Force Research Laboratory
Human Effectiveness Directorate
Directed Energy Bioeffects Division
Optical Radiation Branch
Brooks City-Base, TX 78235-5128

10. SPONSOR/MONITOR'S ACRONYM(S)

11. SPONSOR/MONITOR'S REPORT NUMBER(S)
AFRL-HE-BR-TR-2007-0050

12. DISTRIBUTION / AVAILABILITY STATEMENT
Approved for Public Release, Distribution unlimited. Other requests for this document shall be referred to AFRL/HEDO, 2624 Louis Bauer Drive, Brooks City-Base, TX 78235.

13. SUPPLEMENTARY NOTES
Contract Monitor – Lt Alan J. Rice

14. ABSTRACT

Many infrared (IR) laser systems are being used in tactical military ground and airborne applications. Understanding the biological impact of IR laser energy absorbed by skin and ocular tissues is essential for developing models that can predict collateral hazards. Due to the lack of IR wavelength-dependent microscopic cross sections for skin, research is needed to understand biological damage caused by IR radiation in tissues. Florida International University (FIU) carried out a series of experiments on 34 biological skin samples to measure transmission, reflectance and absorption of IR lasers at 1064 and 1313 nm. Tissue samples varied in thickness from millimeters to microns. Readings from three IR detectors were used to calculate the diffuse reflectance, diffuse transmittance, and collimated transmittance. These values were entered into an Inverse Adding Doubling program to calculate the tissue's optical properties. The results varied as much as an order of magnitude from published results. A secondary goal of this research was for FIU to gain experience in preparation, handling, and measurement of IR in tissues to become a future resource to the U.S. Air Force.

15. SUBJECT TERMS
optical properties, lasers, near-infrared, skin tissue, tissue thickness, computational modeling

16. SECURITY CLASSIFICATION OF:			17. LIMITATION OF ABSTRACT	18. NUMBER OF PAGES	19a. NAME OF RESPONSIBLE PERSON
a. REPORT	b. ABSTRACT	c. THIS PAGE			19b. TELEPHONE NUMBER *(include area code)*
Unclassified	Unclassified	Unclassified	SAR	86	

Standard Form 298 (Rev. 8-98)
Prescribed by ANSI Std. Z39.18

Distribution A – Approved for public release; distribution unlimited

This page intentionally left blank

Table of Contents

Figures

Tables

Acknowledgments

The authors acknowledge the support of the Optical Radiation Branch of the United States Air Force Research Laboratory via contract, F41624-02-D-7003, Task Order 009, awarded to Northrop Grumman Information Technology.

This page intentionally left blank

Executive Summary

Test setups were developed to obtain the optical properties of postmortem Yucatan mini-pig skin in the near infrared (NIR) between the wavelengths of 1 and 2 microns. Two illumination sources were used: a monochromator and lasers at 1064 and 1313 nm. The experimental set up included the following components: a radiation source, two integrating spheres, and three lead-sulfide detectors. The detector signals were processed by a lock-in amplifier and sent to a computer which recorded multiple readings for each test. Tissue samples were tested ranging from full thickness (several millimeters), to the millimeter range, to the micron thickness range. Readings from the three detectors were processed to calculate the diffuse reflectance, diffuse transmittance, and collimated transmittance. These values were then entered into an Inverse Adding Doubling program to calculate the optical properties of the tissue.

The tests with the full-thickness skin samples were performed early in the project using the monochromator. Due to the high attenuation of the beam by the tissue and the low throughput of the monochromator, it was not possible to obtain values that were beyond the noise values of the sensors. Even when using thinner tissue, the sensor values were in the noise range. Changing the wattage of the illumination source to 600 W was still not sufficient to improve the sensor readings. However, when using lasers, it was possible to obtain readings above noise levels and these measurements were processed.

A total of 34 samples were extracted from postmortem Yucatan mini-pig skin and tested using lasers. Some of the tissue was thin epidermal slices (10 and 20 microns thick), while other were approximately 1 mm thick. The thicker tissue used both epidermal tissue (dark-colored tissue), and dermal tissue (light-colored tissue). Based on this setup, the values for the absorption and scattering coefficients for the thin tissue was an order of magnitude above published data. However, the results for the thicker tissue were on the order of published values and relatively similar to the properties of human dermis.

In addition to the optical property experiments, several methods were evaluated to determine the thickness of the sample across the multiple orders of magnitude range of thicknesses used in this project. These methods included measurements using a micrometer, optical microscope, laser profilometer, confocal microscope, and atomic force microscope measurements. For thick tissue, the micrometer method was the easiest, with relatively good accuracy, although care must be exercised to avoid compressing the sample during the measurement process. The optical method can also be used, provided there is sufficient illumination to clearly delineate the edges of the tissue. The laser profilometer method was not able to properly image the dark tissue, although it was able to provide results for light tissue. However, the results for the light tissue were significantly in error. The confocal microscope proved difficult to use due to the subjective nature of determining when a certain depth of the sample was in focus. By using a phosphate solution on the sample, it was easier to obtain repeatable measurements. Finally, the atomic force microscope method shows potential as a technique for measuring thin tissue.

This page intentionally left blank

1. Introduction

The interaction of radiation with tissue is of great importance to the U.S. Department of Defense (DoD) and the medical/biomedical field. The use of infrared (IR) lasers in the tactical military environment (on the ground, at sea, and in the air) presents eye and skin hazards to personnel. Many medium-power laser systems are being used in tactical military ground and airborne applications, including range finding, target designation, ordnance guidance, and night vision illuminators for covert detection, identification, and surveillance. Moreover, lasers have been used offensively against U.S. military pilots and even commercial pilots to inflict temporary or permanent blindness.

In the medical field, the optical properties of biological tissue are important in developing and using many imaging techniques and performing diagnostic studies of the human body and many other biological species. As such, it is revolutionizing modern medicine, allowing non-invasive examination of organs within the human body. Therefore, it is important to study the optical properties of tissue to understand various types of interactions between electromagnetic energy and biological tissue.

Understanding the biological impact of laser energy absorbed by skin and ocular tissues is essential for developing models that can predict collateral hazards from these lasers for various uses or missions. In addition, data from these studies are critical for validation of the modeling and simulation tools used to develop these predictions. Independent of specific applications, it is important to understand how light (UV, visible, and IR) interacts with tissue and what biological reactions are induced. In order to model and simulate possible biological damage caused by radiation in the IR spectrum, it is necessary to perform basic research on processes such as absorption, scattering, transmittance, refractive index, and thermal lensing in tissue samples. In particular, there is currently limited research on the optical properties of tissues at laser wavelengths in the IR spectral region of 1.0 to 4.0 μm compared to the well-studied ultraviolet (UV) and visible spectra.

In order to study the interaction of IR radiation with biological tissue, Florida International University's (FIU's) Applied Research Center, ARC, (formerly the Hemispheric Center for Environmental Technologies or HCET) performed experiments and modeling using IR sources and postmortem biological tissue. The project had multiple goals and tasks. A main goal was to obtain optical properties for biological tissue at IR wavelengths in the 1-2 micron band and to apply an analytical model to determine the optical properties based on the experimental results. A secondary goal was to examine issues related to the testing, handling, and measurement of tissue samples. This goal was added to the original scope of work, and the project end date was extended to accommodate the added goal. This new goal was added based on the availability of a cryostat-microtome that was donated to FIU towards the end of the project. The microtome allowed for sectioning of thin samples (on the order of microns); however, using such a system required additional research and experience in techniques for handling, mounting, and measuring such thin and delicate tissue. A final overarching goal of the project was to improve FIU capabilities in handling and testing biological tissue to become a useful future resource to help the U.S. Air Force address experimental needs in this area. This project final report includes the results for the tasks associated with this research effort along with conclusions and suggestions for improvement in the methods and techniques used throughout the project.

1.1 Background on Optical Properties of Biological Tissue

Biological tissues are inhomogeneous and structurally complex. In the case of skin, the tissue is stratified with several layers. Thus biological tissue acts as a highly scattering medium for radiation in the visible and infrared wavelengths. The majority of light scattering in tissue is due to variations of the index of refraction or mismatched boundaries. In general, scattering in tissues on the microscopic level is attributed to the aqueous-lipid membrane interfaces surrounding each cell [1, 2]. Due to the intricate nature of the skin, it is a challenging problem to determine the major contributors to scattering. In fact, all cellular and intracellular components contribute to the scattering properties of biological tissue. Adding to the complexity is the stratified nature of skin, in which the morphology of each skin layer is unique.

Collagen is the major constituent of skin [3, 4]. Collagen bundles are tightly packed and less abundant in the reticular dermis, as compared to the other skin layers. The collagen fibers in the papillary dermis are smaller and are more sparsely distributed as compared to collagen fibers in the reticular dermis. The collagen fibers in the papillary dermis have a diameter of approximately 0.3 μm – 3 μm, as compared to collagen fibers located in the reticular dermis of the skin, which have a diameter of 10 μm – 40 μm. Microfibrils, a fibrous component of collagen that is embedded in a matrix interwoven with the collagen fibers, are of 10 μm –12 μm in diameter. Because collagen makes up nearly 80% of the dry weight of skin, it is generally assumed that it is the predominant scattering agent in the skin [3, 4].

Light propagation through media such as skin tissue depends on several factors, as shown in Figure 1. Reflection, refraction, absorption and scattering [5] are interactions of photons within tissue that either removes the photon (absorption) or lowers its energy and changes it angular direction. Transmittance is measured as a fraction or percentage and represents the number of photons hitting a detector after traversing a tissue sample over the number of photons hitting the detector with the tissue sample removed. If a tissue sample is too thick or the intensity of the IR radiation source is too low, then optical properties studies are not possible since noise exceeds the signal from transmittance in the detector.

Reflection is the back-scattering of electromagnetic radiation by the incident tissue surface and occurs mainly due to the mismatch of the index of refraction between the air-tissue interface. A second contributor to reflection is called internal reflection. In this type of reflection the incident light penetrates the medium and reflects from inside the medium.

Refraction is related to the difference in the speed of light in one medium relative to another medium. Light changes speed in different mediums due to the changes in the electromagnetic properties of the mediums. This results in a change in the direction of light when it enters different mediums. This sudden change in direction is also responsible for some of the scattering properties of any given turbid medium, including human tissue.

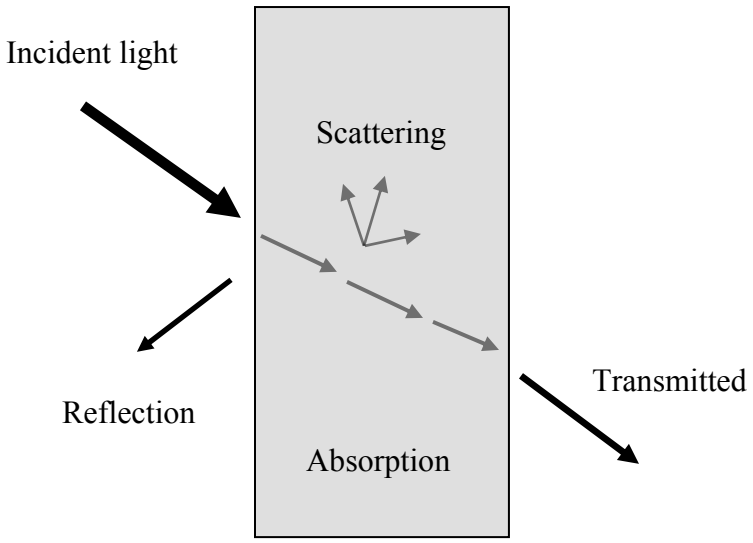

Figure 1. Geometry of reflection, refraction, absorption, scattering and transmittance.

Scattering is the effect of the tissue on the direction of each of the incident photons of a beam. Scattering in biological tissues is mostly elastic (i.e., the frequency of scattered light is the same as that of the incident light) and occurs due to the inherent heterogeneity of media. There are two types of scattering phenomena: independent and dependent scattering. Independent, or single scattering, refers to scattering resulting from interaction with a single particle, whereas dependent scattering is scattering caused by multiple particles. In this context, a particle is used to define any region with a refractive index different from the surrounding area. There are three types of single scattering: Rayleigh scattering, Mie Scattering, and Phase function-dependent scattering events.

Rayleigh scattering occurs when particles are much smaller than the wavelength of the incident light. In Rayleigh scattering there is equal scattering in both the forward and backward directions. Mie scattering occurs if the particle size is approximately equal to the wavelength of the incident light. In Mie scattering, the scattering is predominantly in the forward direction [6, 7]. Collagen fibers of approximately 2.8 μm in diameter have been determined to undergo Mie scattering in the IR, whereas smaller scale collagen fibers undergo Rayleigh scattering [8].

The scattering phase function is used to describe the angular dependence of scattering. The Henyey-Greenstein function is commonly used to represent the influence of anisotropy, or angular dependence, in light scattering [9] as shown in equation 2-1:

$$p(\theta) = \frac{1}{4\pi} \frac{(1-g^2)}{(1+g^2-2g\cos(\theta))^{\frac{3}{2}}}, \qquad (1\text{-}1)$$

where g is the mean cosine of the scattering angle, $g = \langle \cos\theta \rangle$ (also known as the anisotropy factor) and θ is the angle between directions of the incident and scattered photon. Isotropic scattering has an anisotropy factor of zero ($g = 0$), purely forward scattering is characterized by

an anisotropy factor of one (g = 1), and purely backward scattering has an anisotropy factor of negative one (g = -1). For biological tissue (which is forward scattering) the tissue volume has randomly distributed scatterers and thus lacks spatially correlated structures [10]. In such a case, slightly forward scattering can be represented by the first two moment of the phase function as:

$$p(\theta) = \frac{1}{4\pi} \cdot [1 + 3g(\cos(\theta))] . \qquad (1\text{-}2)$$

If a particle is small compared to the wavelength of incident light, there is not much variation in scattering due to direction. This is due to the fact that the wavelets are in phase with each other. The phase relations for the scattered wavelets depend on scattering direction, size of the particle, and shape of the particle [6]. Consequently, as particle size increases, the phase relations tend to become distorted and this causes a disruption in the scattering pattern. Single scattering is indeed a simplification of the scattering phenomena. This simplification takes into consideration a small number of particles with a sufficiently large separation between them. This assumption implies that the total scattered field is the sum of the fields scattered by individual particles. Biological tissue is complex and has variation in size and shape. Single scattering in effect is an idealization strictly realized only with a single object excited by an infinitely distant source. Therefore, in order to better understand light scattering in biological specimens, it is important to consider multiple scattering events.

Multiple scattering, as opposed to single scattering, refers to successive scattering of radiation within the medium. For any given medium, scattering is quantified by the scattering coefficient, μ_s, which is given in units of inverse length (e.g., centimeters, meters, etc.). The probability of transmission *T(z)* of a photon through a tissue section of thickness z without redirection is

$$T(z) = e^{-\mu_s z} . \qquad (1\text{-}3)$$

Therefore, single scattering can be obtained from very thin tissue with a thickness on the order of, or smaller than, the scattering coefficient. A highly scattering medium will make the photons change directions more often. The overall amount of scattering depends not only on the medium but also on the wavelength of the incident light. In any medium, scattering can be traced as a series of events that result in different translations of the photons.

In order to predict the trajectory of an incident photon it is important to determine the number of scattering events as well as the most probable direction of the individual scattering event (i.e., using the scattering phase function). Programs that simulate the trajectory of photons using probability distributions through large number of samples (photons), called Monte Carlo simulations, depend on the values of g and μ_s to predict the trajectory of millions of photons.

Another important effect of a medium upon incident radiation is absorption. Absorption is the process in which radiant energy is absorbed or taken up by a substance. General absorption occurs if the medium, through which radiation is propagating, reduces the intensity of all wavelengths of light by the same amount. In contrast, selective absorption occurs when the media absorbs certain wavelengths of light as compared to others [7, 11]. Biological tissues undergo selective absorption. During absorption, the attenuation of the beam results in a transfer of energy to the tissue which is sometimes detected as heat, fluorescence or by other photo-excitation effects. Absorption is quantified through the absorption coefficient μ_a in units of inverse length. When absorption is much greater than the scattering in a medium, the medium is

considered to be a pure absorber. In this medium light is attenuated by absorption and follows Beer-Lamberts Law:

$$I(z) = I_o e^{-\mu_a \cdot z} , \qquad (1\text{-}4)$$

where I is the radiance at z, I_o is the incident radiation, μ_a is the absorption coefficient, and z is the path length the radiation travels within the medium [1]. The process of light absorption in biological tissue is primarily due to the numerous absorbers present.

The natural absorbers present in tissue are water and tissue chromophores that include certain cellular pigments. The natural chromophores present include the biological pigments—specifically the heme pigment of hemoglobin, myoglobin, and bilirubin [12]. The main tissue chromophores in the infrared region are lipofuscine, xantophyll, melanin, oxyhemoglobin, and deoxyhemoglobin [2, 13, 14]. Beer's Law provides a macroscopic description of light absorption in media, where the intensity of the radiation decreases exponentially along the path of propagation. This model describes energy absorption by particles, but does not account for scattering or emission by particles. Thus, Beer's Law can not be used for scattering media and is unsuitable for thick media such as biological tissue. However, radiative transfer theory can be used to account for such a medium where light scattering and absorption are both present.

By knowing the absorption and scattering coefficients along with the single scattering phase function or anisotropy factor (μ_a, μ_s and g) of a medium for a given wavelength, it is possible to describe the behavior of light in scattering media such as biological tissue [15, 16]. There are two types of experimental techniques employed to measure these microscopic properties: Indirect techniques, and direct techniques [2, 17, 16, 18, 19].

Optical property determination via direct techniques requires that the tissue sample be optically thin (i.e., the sample must display single scattering events). Typically, this requires that the tissue sample thickness be less than the mean free path of an IR photon in the tissue. For soft tissues, this mandates a sample thickness on the order of a micron or less. Direct techniques do not depend on any specific model in order to obtain optical properties. These techniques are in fact, independent of such models. The *in vitro* measurements of the tissue's unscattered light transmission, effective attenuation measurements, and goniophotometric measurements are all that are required to determine the optical properties [2, 16, 18, 19]. However, while optical property determination by the direct method is simple in theory, it can be quite cumbersome and difficult in practice. The sample thickness poses a major problem. As noted before, the tissue thickness must be less than the mean free path. In order to prepare such a thin tissue sample, freezing and subsequent sectioning of the tissue sample must be done. Moreover, cutting and handling such a thin section is very difficult. Another common practice is to homogenize tissue samples to a semi liquid state. These procedures may cause some alteration in the tissue optical properties [2, 4, 8, 14]. For this project, an indirect or analytical method was used for the determination of the tissue optical properties.

Analytical methods to measure optical properties relate measured transmission and reflection values to the optical properties [2, 15, 18]. In this project *in vitro* measurements of reflection and transmission are entered in a light propagation models to determine optical properties. Discussions on the analytical model and experimental setup are included in the next section of this report.

1.2 Modeling

Experimentally determined reflectance and transmittance values can be used to obtain the optical properties (i.e., μ_a, μ_s and g) of a turbid media such as biological tissue. The analysis of this data is based on radiative transport theory. The fundamental basis of the photon transport theory resides in the differential equation for radiance called the radiative transport equation [20]:

$$\frac{dI(\vec{r},\hat{s})}{ds} = -\mu_t I(\vec{r},\hat{s}) + \frac{\mu_s}{4\pi}\int_{4\pi} p(\hat{s},\hat{s}')I(\vec{r},\hat{s}')d\Omega', \qquad (1\text{-}5)$$

where $I(\vec{r},\hat{s})\left[\frac{W}{m^2 sr}\right]$ is the radiation density at a point r in the direction s, $p(\hat{s},\hat{s}')$ is the scattering phase function, which describes the directional distribution of scattered photons. $d\Omega'$ is the unit solid angle in the direction s'. μ_t is the attenuation coefficient given by $\mu_t = \mu_{s+}\ \mu_a$, where μ_s and μ_a are the scattering and absorption coefficients, respectively.

Many approaches for resolving photon transport theory are derived from this fundamental equation. The derived methods that are widely used today are the Kubelka-Munk Theory [1, 21, 22], First Order Scattering Equations, Diffusion Approximation, Monte Carlo simulations [16, 24] and Inverse Adding Doubling (IAD) [24-27]. The method of analysis used for this project was the IAD Method.

1.2.1 Inverse Adding Doubling Method (IAD)

The Inverse Adding Doubling Method (IAD) is based on the so-called "forward solution" to the transport equation using the Adding Doubling Method (ADM) [24-26]. The ADM is a numerical solution to the transport equation whereby reflectance and transmittance values for turbid media can be calculated based on the optical properties. The IAD is the "inverse solution" which iteratively generates improved values for the albedo (a), optical thickness (τ) and anisotropy (g) from which the absorption and scattering coefficients are computed using the ADM and then compares the resulting reflectance and transmittance values to those entered by the user [15, 16, 18, 23, 24]. The IAD method provides for the rapid and accurate solution of inverse scattering problems [16]. The primary advantages of IAD over other methods used to determine optical properties are accuracy and decreased computation time in modeling mismatched boundary conditions and anisotropic scattering events.

The doubling method was first introduced by van de Hulst in order to solve the radiative transfer equation for a specific geometry [24]. The advantages afforded by the ADM are: physical interpretation of results can occur at each step, and the method can be used for isotropic and anisotopic scattering. The disadvantages of ADM are that the calculation of internal fluences in the tissue is not efficient, uniform irradiation must hit the sample, and each layer is assumed to have homogenous optical properties. The latter two disadvantages place restrictions on the sample geometry, that is, samples must be uniformly illuminated and consist of homogenous slabs. The doubling method operates on the following assumptions: the distribution of light is independent of time, samples have homogenous optical properties, sample geometry is an infinite plane parallel slab of finite thickness, the tissue has a uniform index of refraction, internal reflections at the boundaries are governed by Fresnel's law, and the light incident upon the sample is unpolarized [2, 24].

The reflection and transmission for an arbitrary slab are calculated by first determining the reflection and transmission for a thinner slab. This thinner slab should have the same optical properties. In order to ensure that the two slabs have the same optical properties, the thinner slab must be single scattering (i.e., it must be optically thin). Given a slab of specific thickness, thinner slabs are used and doubled until the appropriate thickness is reached. The adding method extends the utility of the doubling method to dissimilar slabs.

The IAD was implemented in C code by Scott Prahl [27]. The source code was downloaded, compiled, and executed for each of the test cases. The experimental setup used for some of the testing had the tissue exposed directly to the IR radiation with no microscope slides, while other samples were supported by one microscope slide behind the tissue. The source code assumed that the tissue was sandwiched between two materials. However, by allowing the user to enter the index of refraction of the front and rear material (along with the attenuation for those materials), the author has made a provision for eliminating either or both of the slides by entering the same index of refraction as air.

1.2.2 Monte Carlo Method

Monte Carlo simulations can be used to describe the propagation of light throughout turbid media. The method is based upon the numerical simulation of photon transport in scattering media. The random migrations of photons are traced throughout a sample from input to output [16, 23, 24]. Monte Carlo simulations provide highly accurate solutions to the radiative transfer equation, however require a major effort to set up and thus were not utilized in this smaller-sized study.

1.3 Thickness Measurements

In order to use the IAD method, it is necessary to accurately measure the thickness of the tissue. To illustrate the sensitivity of the optical properties to the tissue thickness, the IAD method was used with some test constant values for reflectance, transmittance and index of refraction. By entering several tissue thickness values as input to the program, it was possible to show how changes in thickness measurements affected the optical properties. Figure 2 shows a plot of optical properties vs. thickness. The thickness was varied in 10 micron intervals. The plot shows that for thick tissue sections, the optical properties are insensitive to variations in tissue thickness. However, for thin sections (<50 microns) the thickness starts to become important and for thinner sections, there is great sensitivity to changes in tissue thickness.

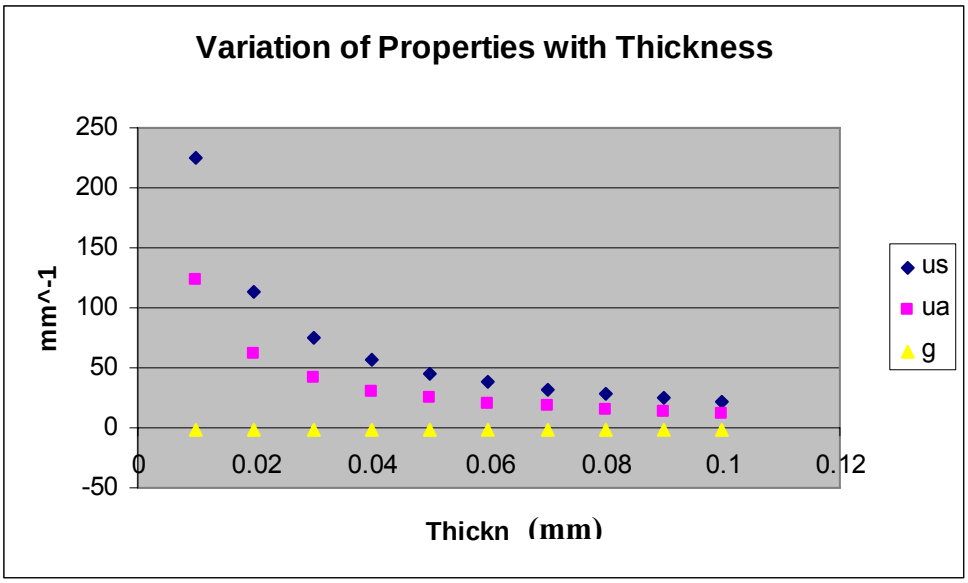

Figure 2. Optical properties vs thickness of skin tissue sample (calculated with IAD).

The results for the anisotropy factor, *g,* was expected because *g* does not change with tissue thickness. This should be the case since the direction of a single scatter doesn't depend on the thickness. On the other hand, absorptive and scattering coefficients vary significantly. The larger thickness means more absorbers and scatterers are present. For constant input values, the IAD method produces constant albedo and optical depth values. Since the absorption and scattering coefficients are inversely related to combinations of these values, as the sample becomes thinner, the mathematical effect of taking the inverse of a small number is magnified, as shown by the figure.

Since tissue thickness measurements create a major factor of error when measuring the optical tissue properties of thin layers of skin, it is necessary for these measurements to be precise enough for an accurate analysis. We have evaluated different tissue thickness measurement methodologies as part of this project.

2. Experimental Setups

An experimental setup was devised to measure the reflectance (R_d), the uncollimated transmittance (T_d) and the collimated transmittance (T_c) of the tissue sample. Originally, FIU proposed the test setup shown in Figure 3 below.

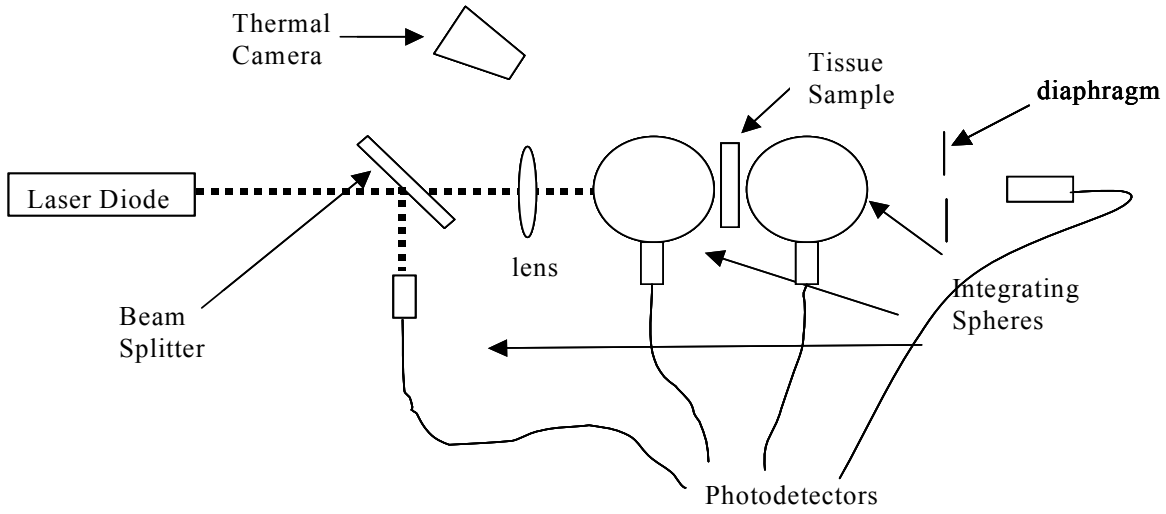

Figure 3: Original test setup.

This setup was based on the use of laser diodes as the illumination source, two integrating spheres for measurement of the diffuse reflectance and transmittance, and a third detector to measure collimated transmittance. A thermal camera was proposed to evaluate changes in tissue temperature as the test progressed. In discussions with the Air Force Research Laboratory (AFRL), and Northrop Grumman scientists, it was suggested that additional test setups be devised for using a monochromator and for directly measuring the anisotropy factor. This led to the following additional two test setups shown in Figures 4 and 5.

While the three test setups and variations on the setups were prepared for testing, useful data was only obtained from a slight modification of the original setup (discussed below). In particular, the anisotropy setup was not used due to theoretical considerations, since the tissue samples were thick enough to cause multiple scattering rather than single scattering of the incident photons.

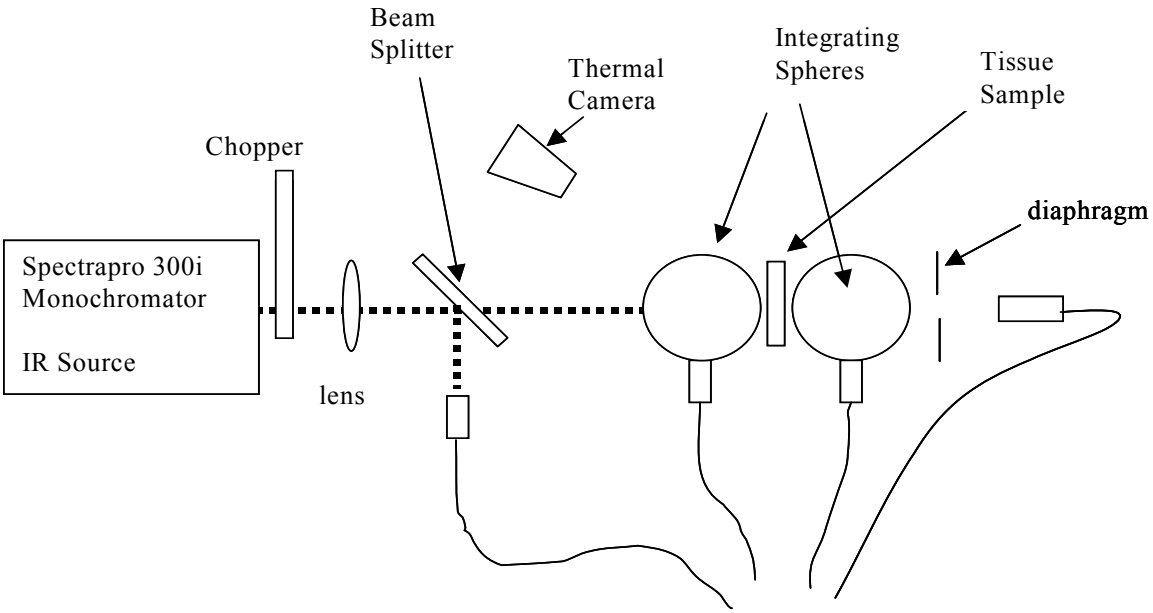

Figure 4. Monochromator test setup.

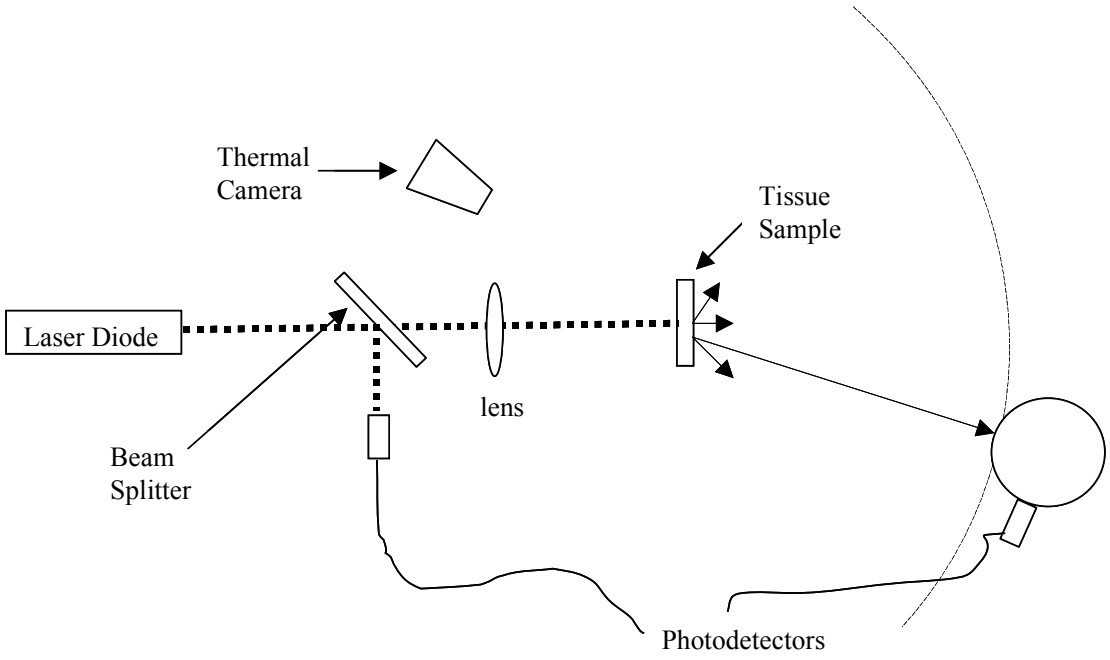

Figure 5. Test setup for direct measurement of anisotropy.

2.1 Optical Properties Test Setup

2.1.1 Integrating Spheres and Radiometry Concepts

This experiment made use of two integrating spheres. The function of the spheres was to spatially integrate radiant flux and act as ideal optical diffusers. Thus, the spheres provided uniform illumination to the detectors, thereby facilitating reflectance and transmission measurements. The interior of the spheres was coated with BaS_2, to provide a surface with high reflectance in the IR region of interest (1 to 2 μm). The spheres have baffles to prevent radiation from the tissue from entering the detectors directly.

During the experiments, IR radiation entered the first integrating sphere via the entry port and traveled through the exit port where it then encountered the tissue sample in the tissue holder. Radiation from the tissue is diffusely backscattered into the first integrating sphere and forward scattered into the second integrating sphere. The radiation is uniformly reflected and scattered within the spheres where detectors measure a portion of the radiation. Radiation that remains collimated (i.e., unscattered) exits the second integrating sphere and travels to the collimated transmittance detector. One of the main disadvantages of the integrating spheres is that the radiation is spread throughout the surface of the sphere and only a small portion enters the detector. This could result in a nearly 1000 to 1 reduction in signal strength based on the surface area of the sphere vs. the area of the detector, which could result in detector signals that are at or near the noise values. Increasing the energy of the incident radiation may not always be an option, since that could lead to damage to the tissue. Another effect that occurs when using two integrating spheres is cross-talk between the spheres [28]. The cross-talk occurs when light from the second sphere reflects back through the tissue to the first sphere and vice versa. During the process, the radiation travels through the tissue so its effects are attenuated. Nevertheless, there would be some slight additional absorption of energy by the tissue in this configuration.

2.1.2 Equipment

The collimated beam from the IR source was split to provide a reference beam using a beam splitter (Oriel/ Spectra-Physics/Newport Model 45700). Tests of the beam splitter indicated that both the front and rear surfaces of the splitter were reflecting and transmitting part of the beam resulting in a double-peaked beam, which was undesirable. Therefore, the beam splitter was not used in subsequent testing. However, the value of the incident beam was measured as part of every experiment using the collimated transmittance detector, with no tissue in place, to account for drifting or variation in the intensity of the illumination source.

The integrating spheres used for the test were Oriel/Spectra-Physics/Newport general-purpose integrating spheres (Model 70451). These spheres are 152 mm in diameter (6 inches) with three 33mm apertures. The reflectivity of the spheres decreased with wavelength but was adequate for the one to two micron wavelength range.

The detectors were factory-calibrated Oriel/Spectra-Physics/Newport Model 70343 lead sulfide (PbS) detectors. PbS detectors are well suited for the IR radiation region. The specifications for these detectors are shown in Table 1.

Table 1. Specifications for the lead-sulfide detectors.

Detector	Area (mm^2)	Voltage Gain	Response Time (µs)	Amplifier (V)	Bias (V)
PbS	9	2, 10, 50	400	15	5

These detectors have an accurate detection performance, fast response as compared to other detectors, and are operable at room temperature. Moreover, the detectors mate perfectly with the ports of the integrating spheres. The detectors connected to the integrating spheres were set at maximum gain (50x), while the collimated transmittance detector was set at the minimum gain (2x).

In order to accurately measure infrared output, an IR digital lock-in radiometry detection system was utilized (Oriel/Spectra-Physics/Newport Merlin Control Unit with RS232 com port – Model 70100). This lock-in amplifier has an internal 2-pole filter, auto-ranging gain, and an RS232 output. The radiometry system works in conjunction with a closed optical chopper (Oriel/Spectra-Physics/Newport Model 75152 with chopper wheel Model 75162) and the PbS detectors to process the signal and present it as either a voltage, or ratio of voltages (signal voltage/reference voltage). The optical chopper modulated the radiation that entered the integrating spheres, thereby allowing the radiation to be read by the PbS detectors. The process of chopping helped to reduce ambient noise and power line noise. In order to determine the best chopping frequency, the detector type and configuration must be taken into consideration. During our testing, it was determined that chopping near 9 Hz produced the lowest noise values in the detectors. In order to hold the samples in place for measurement, a custom tissue holder was devised.

The tissue holder was a custom system that can be easily replicated. It consisted of a 38 mm (1.5 in) diameter lens holder (Oriel/Spectra-Physics/Newport Model 6195) along with two 11 mm (0.437 in) diaphragms (see Figure 6). The lens holder contained a threaded ring that is normally used to hold the lens in place. This ring was still used, but an aluminum cylindrical spacer of 38 mm OD, 28 mm ID, and 8 mm thickness was made to help hold the tissue and decrease the amount of revolutions needed to tighten the threaded ring.

Figure 6. Custom tissue holder.

Thick tissue sections were sandwiched in between the two 11mm diaphragms to provide an air-tissue-air interface. However, the thin tissue sections were so fragile that they had to be mounted on a glass slide for structural support. The slides were cut to fit the tissue holder and the tissue was oriented such that the IR radiation encountered air-tissue, tissue-glass, and finally glass-air interfaces.

To monitor the temperature of the tissue sample, an Indigo Systems TVS-700 infrared camera was used. This camera is sensitive between 8 and 14 μm and has 320 x 240 detector elements. The minimum temperature resolution for this camera is 0.08°C. Some before/after IR images were taken to monitor changes in tissue temperature. Since the power used on the tissue was relatively low, there was no significant heating of the tissue measured during initial tests. Therefore, no additional measurements were collected on the temperature change in tissues during the tests.

2.1.3 Monochromator Setup

The monochromator setup, previously shown in Figure 4, was based on a Spectra Pro 300i monochromator, which was already owned by FIU. To use this monochromator in the IR region of interest, a new diffraction grating with 600 g/mm, 1.6 μm blaze (Acton Research Model I1-060-1.6) was purchased and mounted on the grating turret. Software that came with the monochromator allowed for the selection of a given grating and wavelength. The light source for the monochromator was a quartz-tungsten 100 W radiation source (Oriel/ Spectra-Physics/Newport Model 6333), mounted in a lamp holder. Later, a 600 W quartz-tungsten halogen lamp was also used (Oriel/Spectra-Physics/Newport Model 6333). The entrance slit to the monochromator was opened as wide as possible (3 mm) while the exit slit was adjusted to a 1mm aperture to produce a 6 nm wavelength spread. The height of the exit slit was 14 mm but was reduced to 3 mm to fit the collimated transmittance detector size. The output beam was collimated with a CaF_2 lens of 37 mm diameter and 152 mm focal length (Oriel/Spectra-Physics/Newport Model 43240). The chopper was mounted such that the chopping action would cut the beam from top to bottom in order to avoid "chirping" the beam. Otherwise, as the chopper edge closes, it would have the same effect as closing the exit slit and changing the beam from a small range of wavelengths, to an even smaller range of wavelengths or no radiation.

The test procedure used with the monochromator in the setup was as follows: first allow the equipment to warm up while the system is aligned. The beam alignment was done by setting the monochromator to a visible wavelength and visually aligning all of the components. By placing targets in a lens holder, and placing the lens holder before and after each integrating sphere, and before the collimated transmittance detector, it was possible to align each element. After alignment, the chopper was turned on at a frequency of 9 Hz. The filter on the lock-in amplifier was set to a 0.3 second time constant. The data acquisition software was started and prepared for data collection. The monochromator was then set to an IR wavelength, and the collimated transmittance detector was moved slightly to ensure final alignment by seeking the maximum value from the detector. After alignment, and warm up of the equipment, the tissue sample was mounted on the tissue holder. The holder was placed between the two integrating spheres, mounted in front of the second integrating sphere. After selecting the desired wavelength, and allowing the detector signal to stabilize, each detector was measured for a time period between 30 seconds and one minute, and the average value was recorded. This procedure was repeated for various tissue samples and wavelengths.

2.1.4 Laser Setup

The original test setup shown in Figure 3 used lasers diodes to generate the incident beam. Laser diodes typically have a high beam divergence and therefore need a collimating lens. The AFRL had several lasers that were available for testing, thus the laser setup used a 1064 nm laser and a 1313 nm laser. These lasers had a small beam divergence so the collimating lens was removed. The 1064 nm laser was a Coherent DPSS (Diode Pumped Solid State) Nd:YAG continuous wave Class IIIb laser. The 1313 nm laser was a diode pumped Nd:YLF, Class IIIb, continuous wave system by Crystal Laser. The laser specifications are shown in Table 2.

To operate the lasers, all personnel had to complete Laser Safety training and obtain a baseline eye test. Standard operating procedures (SOP) were developed for aligning and using the laser system. These procedures were reviewed and approved by the Environmental Health & Safety officer and FIU's Laser Safety Officer.

Table 2. Laser specifications.

Laser	Wavelength (nm)	Power (mW)	Beam Divergence (mrad)	Beam Diameter (mm)
1	1064	500	< 1.8	1
2	1313	170	4.2	0.5

The test procedure when using the laser was similar to the test procedure when using the monochromator. The main difference was in the additional safety equipment and procedures associated with using a laser. The beam was aligned using an IR-sensitive card with final adjustment of the collimated transmittance detector performed by maximizing the reading of this detector.

2.1.5 Final Setup

After trying the different setups, a final test configuration emerged which was successfully used to collect data. This setup was a variation of the original one and is shown in Figure 7. In this final setup, a laser produces collimated IR radiation which was attenuated via a variable-aperture diaphragm and chopped before entering the first integrating sphere and interacting with the tissue. The detector in the first integrating sphere measured the diffuse reflectance. The detector in the second integrating sphere measured the uncollimated (diffuse) transmittance, and the third detector measures the collimated (unscattered) transmittance. Each detector was selected in turn using a selector box. The aperture on the rear diaphragm was 9 mm. A photograph of this test setup is shown in Figure 8.

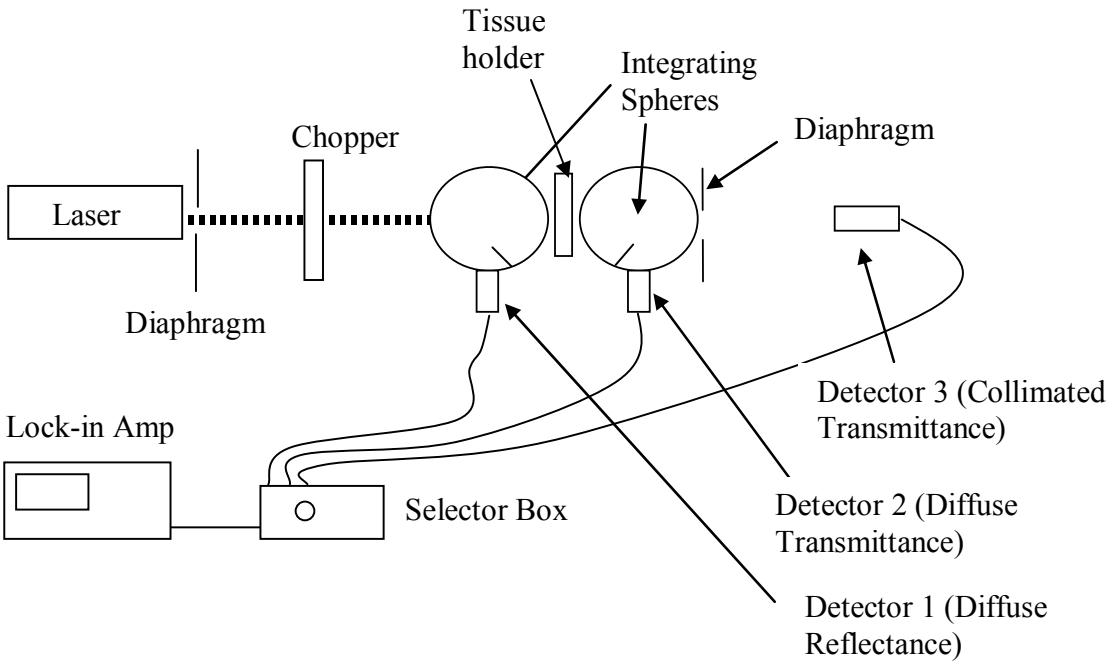

Figure 7. Schematic Diagram of the final laser test setup.

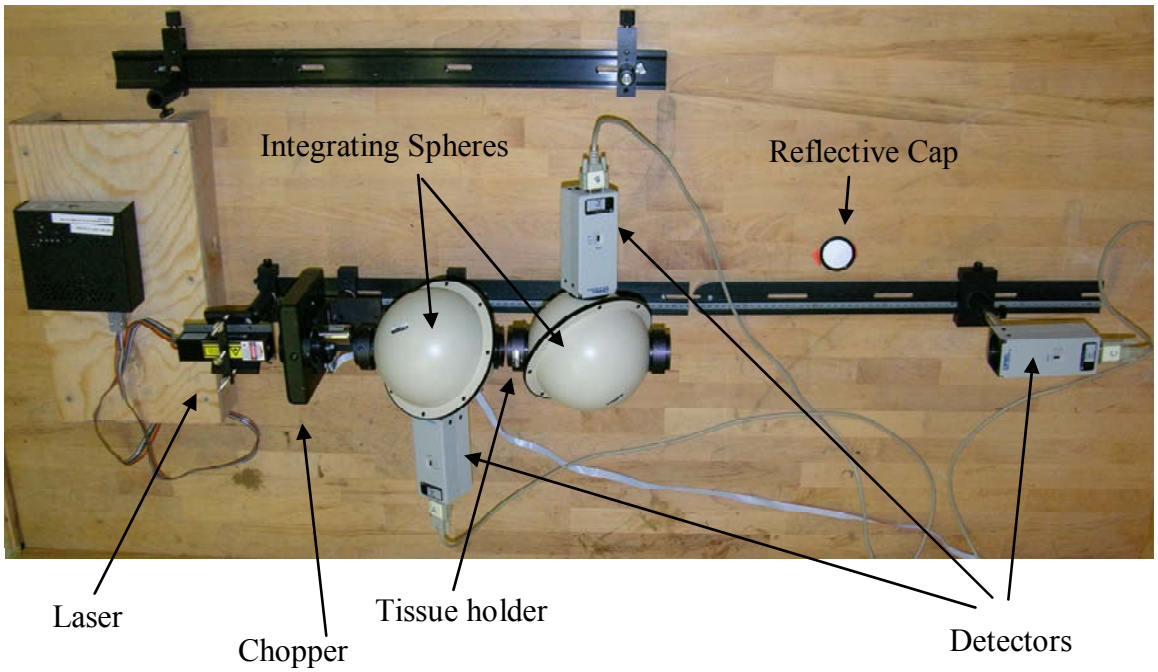

Figure 8. Photograph of the final test setup.

2.2 Data Acquisition/Processing

The lock-in amplifier did not have the ability to collect multiple detector data simultaneously. Therefore, the different detectors were connected to a breakout box that was sequentially switched to capture data from each detector. The data collected from the detectors were processed by the lock-in amplifier and sent to a computer via the RS232 port. A BASIC program was written to interface with the serial output of the lock-in amplifier and collect the data (see Appendix A). The program collected data for approximately 30 seconds resulting in 140-175 individual measurements sent to the computer. During a run, the user entered a file name for storage of the output data. The program paused for approximately 30 seconds to allow the data to stabilize (after switching detectors) and collected data. When complete, the average value of the data was printed on the screen and was manually recorded in a logbook. The raw data was stored for post-processing.

For each tissue sample, the following data was collected: readings from the detector in the first integrating sphere (corresponding to the diffuse reflectance or back-scatter), readings from the detector in the second integrating sphere (corresponding to the diffuse transmittance or forward-scatter), and readings from the third detector (corresponding to the collimated transmittance). Another measurement collected for each test was the intensity of the beam with no tissue in place (i.e., the reading of the collimated transmittance measurement with no tissue in place). This fourth measurement was used to normalize the data and account for changes in the intensity of the incident beam throughout the test period. During the test collection period, the room lights were kept off, since they increased the noise in the detectors.

While these measurements were collected for each tissue sample tested, two other measurements were collected at convenient times during the test (such as at the start and end of the testing session). These measurements were the intensity of the illumination source at each detector, and the noise measured by each detector without the tissue in place but with the sample holder in place and the illumination source on. The intensity measurements for the first and second detector were made as shown in Figure 9.

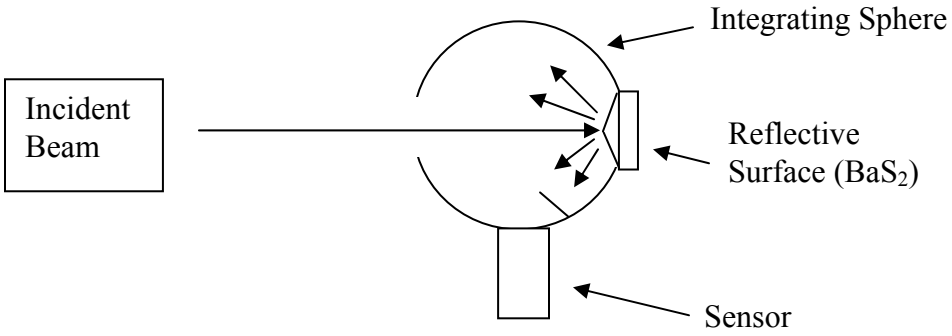

Figure 9. Configuration for measuring beam intensity.

For these measurements, the incident beam from the laser travels through the input port and is reflected at the exit port by a conical reflective cap coated with BaS_2 (same coating as the integrating sphere).

In addition to these measurements, several other measurements were collected to understand the sensitivity of the setup to changes. For example, the noise in the sensors was recorded throughout the different test days to ensure that the sensors were not drifting or deteriorating. Beam intensity measurements were made with and without the tissue holder; tests were done with the tissue mounted in the rear of the first integrating sphere and in the front of the second integrating sphere, etc.

In order to compute the optical properties from the experimental data, it was necessary to convert the raw voltage readings from the sensors into diffuse reflectance, R_d, diffuse transmittance, T_d, and collimated transmittance, T_c. To calculate these values, each raw data file was processed to produce a single mean value (from the 100+ individual measurements made during the collection period), for each sensor, for each test. From the measured values, the diffuse reflectance, R_d, is given by:

$$R_d = \frac{\frac{S_a}{I_c} - \frac{N_a}{I_{on}}}{\frac{I_{oa}}{I_{oc}} - \frac{N_a}{I_{on}}}, \qquad (3\text{-}1)$$

where:

S_a is the signal from the sensor on the reflectance (first) integrating sphere, with the tissue sample in place;

I_c is the intensity of the laser beam detected from the collimated transmittance detector with no sample in place;

N_a is the noise detected from the sensor in the first integrating sphere when the laser is on, the sample holder is on, and there is no tissue in the sample holder;

I_{on} is the intensity of the laser beam detected from the collimated transmittance detector with no sample in place just after the value for N_a was measured;

I_{oa} is the signal from the sensor on the reflectance (first) integrating sphere with no sample in place, and the exit port covered by a reflective cap (as in Figure 9); and

I_{oc} is the intensity of the laser beam detected from the collimated transmittance detector just after I_{oa} was measured and the reflective cap was removed from the exit port of the first integrating sphere (to allow the beam through to the detector).

Similarly, the diffuse transmittance, T_d, is given by:

$$T_d = \frac{\frac{S_b}{I_c} - \frac{N_b}{I_{on}}}{\frac{I_{ob}}{I_{oc}} - \frac{N_b}{I_{on}}}, \qquad (3\text{-}2)$$

where S_b is the signal from the sensor on the transmittance (second) integrating sphere, with the tissue sample in place;

I_c is the intensity of the laser beam detected from the collimated transmittance detector with no tissue sample;

N_b is the noise detected from the sensor in the second integrating sphere when the laser is on, the sample holder is in, and there is no tissue in the sample holder;

I_{on} is the intensity of the laser beam detected from the collimated transmittance detector with no sample in place just after the value for N_b was measured;

I_{ob} is the signal from the sensor on the transmittance (second) integrating sphere with no sample in place, and the exit port covered by a reflective cap (as in Figure 9); and

I_{oc} is the intensity of the laser beam detected from the collimated transmittance detector after I_{ob} was measured and the reflective cap was removed from the exit port of the second integrating sphere.

Note that if the test had been performed such that the sensor readings had been obtained as a ratio between the sensor signal and the beam intensity, it would not have been necessary to divide the numbers by their respective beam intensities, I.

Finally, the collimated transmittance, T_c, is calculated as follows:

$$T_c = \frac{S_c}{I_c}, \qquad (3\text{-}3)$$

where S_c is the signal from the collimated transmittance detector with the tissue in place, and I_c is the signal from the same detector with the tissue removed. By performing the detector noise tests, the values N_a, N_b, and I_{on} were obtained. By performing the beam intensity measurements as per Figure 9, I_{oa}, I_{ob}, and I_{oc} were obtained. Finally, for every tissue sample, S_b, S_b, S_b, and I_c were collected.

The calculated values for R_d, T_d, and T_c, were used as input values to an IAD program. This program calculated values for the albedo (a), the optical depth (τ), and the anisotropy factor, (g). From these values, and the thickness of the tissue (z), it was possible to calculate the absorption and scattering coefficients (μ_a and μ_s), using Equations 3-4 and 3-5.

$$\mu_s = \frac{a \cdot \tau}{z} \qquad (3\text{-}4)$$

$$\mu_a = \frac{(1-a) \cdot \tau}{z}. \qquad (3\text{-}5)$$

In addition to these parameters, the IAD program requires a value for the index of refraction. This parameter is difficult to measure in turbid media (media with absorbers and/or scatterers)

such as tissue, which is why the value is usually approximated by the refractive indexes and concentration of the individual molecules. Tissue consists of approximately 80% water which is why the index of refraction ranges from 1.33 to about 1.60. While the index of refraction varies with wavelength, it is often approximated as 1.4 [29, 30]. This value was used for all IAD calculations in this project. To show that the results were not sensitive to the index of refraction, a fixed value was used for R_d, T_d, and T_c, while the index of refraction was varied between 1.3 and 1.6. The results show little change in the scattering coefficient, a 10% change in the absorption coefficient, and a 3% change in the anisotropy factor.

For samples that required a glass microscope slide for structural support, the index of refraction of the slide was entered as 1.52, with an optical depth of 0.05. Early in the project, these slides were tested and shown to have high transmission in the IR.

3. Specimen Preparation

In this section, we discuss the preparation of the tissue and how samples of different thickness were extracted from the skin. In addition, we discuss the mounting of the tissue along with methods for measuring the thickness of the tissue.

3.1 Tissue Preparation

The animal model used to simulate human skin was the Yucatan mini pig. Previous studies have shown that this breed of pig has skin characteristics very closely related to those of human skin. In order to perform experiments involving animals, protocols were developed and approved by FIU's Institutional Animal Care and Use Committee (IACUC). In addition, since the tissue used in this research was obtained through Miami Children's Hospital (MCH), they also had to submit protocols which were approved by their IACUC.

The skin of the postmortem Yucatan mini pigs was provided by Miami Children's Hospital one day post-mortem. The tissue came as a roughly rectangular piece measuring approximately 18 x 17 cm (see Figure 10). The fresh skin was stored and sealed in a bag with an isotonic solution or nutrient medium at a temperature between 2 and 10 degrees Celsius. A small refrigerator with temperature control and a thermocouple was checked periodically to ensure that the correct temperature range was maintained. During the beginning of the project, experiments were attempted using the full thickness of the tissue. This required shaving the tissue for hair removal (there were approximately 15 hairs per square cm) and removal of the bottom layer of fat. An irregular fat layer approximately 3 mm thick (see Figure 11) was removed using a sharp knife or scalpel. The fat had to be pulled as the cut was made (as though it was going to be peeled off) in order to remove the maximum amount of fat. The remaining tissue was several millimeters thick and was cut into square sections less than 2 cm on each side. Shortly after cutting the tissues they were either testing or stored once again at a temperature of in the 2-10 degrees Celsius range.

Figure 10. Postmortem Yucatan mini pig skin.

Figure 11. Tissue sample with fat layer underneath.

In addition to the full-thickness samples, thinner samples were extracted. The thinner samples were obtained using a Model B, Padgett Electro-Dermatome. The dermatome had a vibrating blade with a side to side motion for cutting the tissue. Guards on the tool determined how wide a piece could be cut. Originally, the tissue was cut by setting the dermatome depth-of-cut lever and using the tool directly on the skin, as shown in Figure 12. However, after further experimentation, it was discovered that the most effective way to cut with the dermatome was to first cut the tissue into strips approximately 1.5 cm wide and as long as the skin sample. Then, individual strips were laid on a support of approximately the same width as the strips. The support could be a thin piece of wood, or a piece of cardboard folded in half, but the idea was to raise the tissue several millimeters above the table. The guard on the dermatome was chosen such that the entire width of the tissue could be cut. This method was used to cut the top layer of the tissue and a second layer underneath. The desired thickness for the tissue strips could be set by an adjustment lever on the dermatome. For this project, the dermatome was used to cut approximately 0.75 mm thick strips with the epidermis and the dermis. These strips were relatively thin, when compared to the full thickness of the tissue; however, they were still easy to handle and resistant to tearing (see Figure 13). The strips were subsequently cut to twelve samples, which were ultimately tested. Six of these samples included tissue with epidermis (dark samples) and the other six were a sub-layer of skin (dermal layer) with all white tissue (see Figure 14).

Figure 12. Use of dermatome on tissue.

Figure 13. Strips cut with the dermatome.

Figure 14. Samples (23-34) ready for testing.

Towards the end of the project, a Tissue-Tek Microtome/Cryostat model 4551A was donated to FIU (see Figures 15 and 16). This microtome could cut thin sections (2 to 20 micrometers) and cool down to –40°C. This instrument was used to cut thin samples at 10 and 20 micron thickness. Tissue samples with a 10-20 μ thickness were extremely fragile, and many cuts had to be performed before an acceptable sample was obtained.

Ten skin sections 1 cm x 1 cm were cut and prepped for fine cutting with the microtome at -20°C (see Figures 17 and 18). Out of the 10 tissue sections, 22 samples were removed with roughly half at 20 micron thickness and half at 10 micron thickness. Generating an acceptable specimen took many cuts with approximately one in 10 being acceptable for testing. Some of the difficulties with obtaining an acceptable sample were due to the thinness of the samples. Such thin specimens are extremely delicate and tear easily. Moreover, cut samples may be too small, or have small holes or tears that make them unacceptable. Samples sometimes curl as they are cut and can be difficult to uncurl without damage (see Figure 19). Curling would occur when the area near the cutting blade was at a slightly warmer temperature than the tissue. Finally, some samples were simply too small to fill the 11 mm diameter hole of the test mount. Even after the initial prescreening, which occurred as the samples were being cut, four of the 22 samples were ultimately not used because they were too small to fill the test mount aperture (see Figure 20). While the IR laser beam was much smaller than the sample size, there was a risk that a slight

misalignment of the system would cause the beam to hit part tissue and part empty space, thus skewing the data. Figure 21 shows a good example of a properly sized sample next to the sample holder (for comparison). Samples from the topmost skin layers had holes due to hair in the specimen. Cuts below the topmost layers were more uniform. In order to ensure flatness of the top surface of the tissue and uniform thickness of the cut, several cuts had to be made of the top layer before obtaining a sample. The prepped samples were stored in a humid bag inside a refrigerator at temperatures between 2 and 10°C. Despite these measures, it was hard to keep the samples from drying out.

Figure 15. Tissue-Tek Microtome/Cryostat.

Figure 16. Alternate view of cryostat.

Figure 17. Samples ready to mount for cutting with the microtome/cryostat.

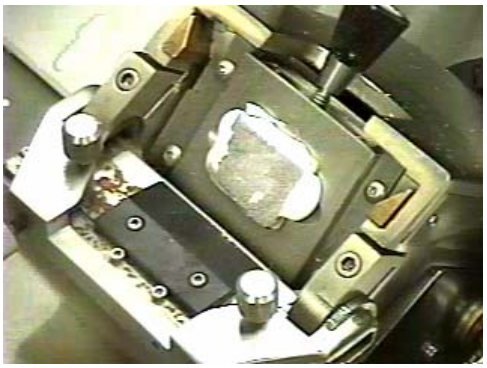

Figure 18. Tissue sample mounted on the microtome/cryostat.

Transferring the cut samples from the microtome to the slides required the proper technique. If too much pressure was applied, the sample stuck to the slide but also to the microtome surface causing tearing of the sample. The best technique was to turn the sample such that it was slightly convex and lightly touching the convex center with the slide. Removal of a sample that was not adequate was best performed by simply using water. Various alcohols were tried but were not efficient in removing the tissue.

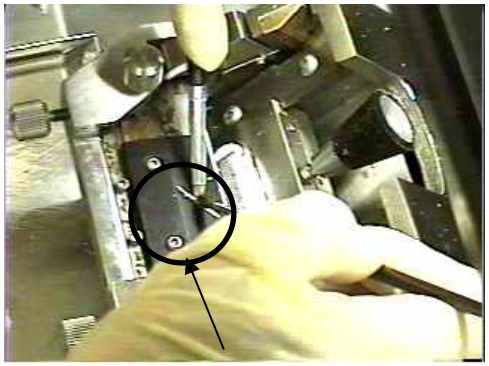

Figure 19. Sample tightly curled after cutting.

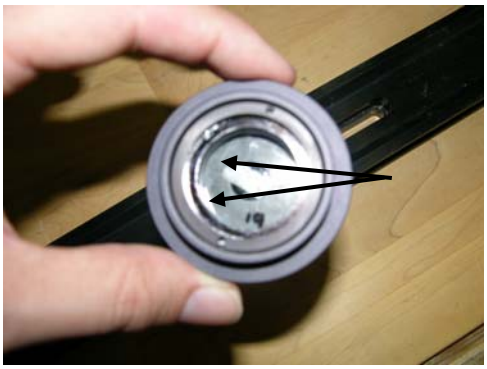

Figure 20. Sample 19 did not fill the sample holder window and was rejected.

Figure 21. Good sample next to sample holder.

3.2 Sample Mounting

Previous experiments have utilized cuvettes as tissue holders. However, due to the delicate nature of the tissue and the potential glass/air interaction, a custom tissue holder was constructed, as described in Section 3.1.2. The samples were mounted between the thin washers that comprise part of the sample holder. The sample holder was tightened only enough to hold the sample in place but not to squeeze the tissue significantly. The sample was examined to make sure it was not wrinkled, slack, nor stretched. The thick samples were mounted without using any glass or slides. Thus, the thick samples had an air-tissue-air interface for the impinging photons. The thin samples were mounted on one slide producing air-tissue, tissue—glass, glass-air interfaces. The glass slides were cut to ensure that the tissue covered the maximum amount of the opening in the sample holder. Before testing, the sample was allowed to reach room temperature (~25°C). Initial sample temperatures were confirmed using an infrared camera. Once the time required for samples to reach room temperature was determined, the infrared camera was used only to provide confidence that all samples had reached room temperature prior to testing.

3.3 Tissue Thickness Measurement Methods

In order to determine the optical properties of the tissue, it is necessary to enter the tissue thickness into the IAD computer model. Several techniques were tested to evaluate and compare

different measurement methodologies. Since the samples varied in thickness by orders of magnitude, different techniques had to be used for different tissue sizes. In particular, the techniques were divided into "thick" tissue measurement methods (for tissue in the millimeter range), and "thin" tissue measurements methods (for tissue in the micron range).

3.3.1 Thick Tissue Measurement Methods

Thick tissue measurements were obtained using three methods: an accurate hand-held micrometer, a laser profilometer, and an optical microscope with video capture capabilities. Several techniques were attempted using each of these methods to determine the best way of making the thickness measurements.

3.3.1.1 Micrometer Measurement Method

One method used to measure the thickness of thicker tissue (on the order of millimeters) was to use a high-accuracy micrometer (shown in the foreground of Figure 22). The micrometer used for the test was a Mitutoyo model 103-135, 0-1" friction micrometer. This micrometer had a resolution of 0.0001" (2.5 microns) with an accuracy of ± 0.0001", and was calibrated prior to use. The diameter of the measuring faces was 0.25", with a flatness of 0.000024" (0.6 microns) and a parallelism of 0.000090" (2.3 microns). This micrometer had a friction thimble that acted as a clutch and slipped when a factory set force between the measuring surfaces was reached.

The method for measuring the thickness of the tissue was as follows. First, both slides were placed in contact with each other and the thickness of the two slides together was measured. Then, the twelve thick samples were measured by placing the tissue between the two microscope slides and measuring the thickness of the entire assembly. The micrometer thimble was turned until it started to slip, and the thickness was read from the micrometer. While performing the test in this fashion, it was apparent that the tissue was compressed due to the force of the micrometer measuring surfaces. Moreover, continued rotation of the thimble would cause slippage for a moment but would later allow for a few more degrees of rotation as the tissue continued to compress. Since the compression of the tissue resulted in a lower reading (i.e., thinner tissue reading), a second technique was utilized.

The second method was similar to the first but did not depend on the slipping of the micrometer thimble. Instead, the micrometer was adjusted until there was contact between the measuring surfaces and the slides. To ensure that there was full contact of the measuring surfaces, the micrometer was pulled in a perpendicular direction to gage the sliding resistance of the micrometer relative to the slides. The micrometer was adjusted until a slight resistance was felt when moving the micrometer (this resistance was similar to the resistance experienced when using a feeler gage and could be described as a light "magnetic" drag.) Since the samples were not fresh (although they had been refrigerated), some of them were slightly curled. Therefore, after mounting the tissue (with water between the slides), the micrometer was used to compress the sample using the first technique, then the micrometer was backed off and the measurement was performed using the second technique. The thickness of each sample was measured and noted in a logbook.

Using the second method, all samples were measured three times. Some samples were also measured with the first method to provide information on the degree to which the tissue was compressed using the first method.

3.3.1.2 Laser Profilometer Measurement Method

A different method utilized to measure the thickness of the tissue was the laser profilometer method. A laser profilometer is a non-contacting profile measurement system based on optical triangulation to determine the distance to a target [31]. The system used for testing was the LTC model LP-2000 laser profilometer with the LP-S-5/2 sensor (see Figure 22). This sensor works with a standoff distance between 50 and 127 mm and has a resolution of 25 microns. The sensor utilizes a red laser as the light source.

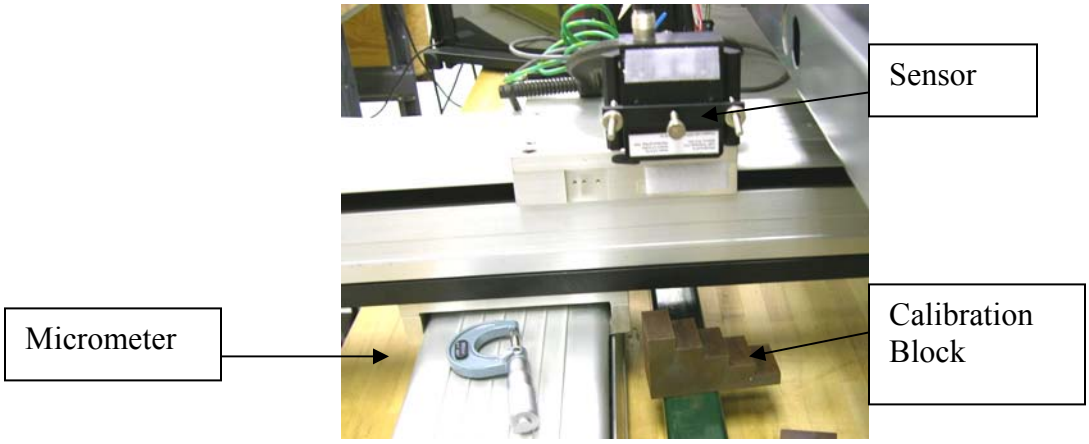

Figure 22. Laser profilometer setup.

The sensor was calibrated using the manufacturer's calibration block. Since this block spans the standoff distance of the sensor, a reference measurement was later made using an object approximately 7.5mm thick (measured with the micrometer) to provide a more precise calibration. The samples were placed on a slide, or a background surface of similar color to the tissue. The sample was moved such that the background distance was measured for four seconds, then the tissue was moved such that the laser targeted the center of the tissue. This position was held for four seconds and the values were recorded.

3.3.1.3 Optical Microscope Measurement Method

A third method used to measure the thickness of thick tissue samples was to use an optical microscope and a computer program that could measure distances of objects through the microscope. The system used was a Wesco Pol VU 6300 series microscope with a color video camera attached to the trinocular head. The image capture and measuring system was a COHU CCD color camera (COHU Inc., model 2222-1340), a 24 bit video capture card (Flashpoint Intrigue Pro-video Card Model 3120) and video measuring/marking software (Boeckeler VIA S200). Measurements were made with a 5X objective lens and a 10X wide-field eyepiece, resulting in an overall magnification of 50X. This combination resulted in a field of view of 1.6 mm horizontal by 1.3 mm vertical.

Calibration of the microscope system was performed using a 27 mm cross scale reticule with 0.1mm markings (Edmund Optics NT39- 450). The linear accuracy of the scale was ±2 microns. The reticule was placed in the microscope field of view and the calibration conversion factor

from screen pixels to linear distance was calculated by the software based on a 1 mm measuring distance. Using this setup and magnification, the minimum resolution of one pixel on the screen corresponded to a linear distance of 3 microns.

To collect thickness measurements, the thick tissue sections were placed between two slides, with part of the tissue just beyond the edge of the slides. The slides were mounted in the microscope vertically, such that the microscope had a clear view of the width of the tissue. The slides were not compressed near the top to not affect the thickness of the tissue (although the slides compressed the tissue in the bottom). The microscope light setting was adjusted such that the light illuminated the specimen from the top. The aperture for the light was adjusted to have a better depth of field. For each sample, an image was captured with the frame grabber. The image was later analyzed to measure the thickness of the tissue.

Since this method imaged the edge of the tissue, which was never perfectly square, it was difficult to see the edges of the tissue without increasing the depth of field. Even then, there was still some difficulty in imaging the lighter tissue, and the method had to be modified.

Due to difficulty in imaging the edges of the dark-colored tissue, the method was modified such that the tissue was mounted on only one slide and imaged in the same manner. To improve detection of the edge, tweezers were used to just touch the tissue and then the image was captured using the frame-grabber. The captured images were later analyzed to determine the thickness of the tissue, with the tweezers providing a more readily visible edge. The tweezers also provided better illumination of the tissue by reflecting some of the incident light towards the tissue. While the measuring system was capable of high accuracy, the determination of the edge of the tissue proved to be the largest contributor to the overall measurement error. The edges were detected from slight shade differences in the image, since it was not possible to clearly focus both edges of the tissue at once. One way to clearly delineate the edges would be to use the microscope slides as the edges; however, it would require additional procedures to assure that the slides were parallel and in contact with the tissue but not compressing it.

3.3.2 Thin Tissue Measurement Methods

Several methods were considered in order to measure the thickness of thin tissue. Due to the thinness of the tissue, typical optical microscopy was not suitable, nor was direct measurement using a micrometer. Possible methods considered were scanning electron microscopy (SEM), confocal microscopy and atomic force microscopy. The SEM method was not used because SEMs work with the specimen under vacuum. This would cause significant dehydration of the tissue and thus decrease the thickness value. However, confocal microscopy and atomic force microscopy work at atmospheric pressure and temperatures, so these methods were attempted as described below.

3.3.2.1 Confocal Microscope

One method used to measure the thickness of the thin specimens (on the order of microns) was to use a confocal microscope to differentially focus through the sample. The microscope used was a Leica ICM 1000 Industrial Confocal Microscope (see Figures 23 and 24). This microscope had options for illuminating the specimen in the UV, visible, and IR spectral range. The system specifications indicate that this system is able to achieve a depth (z-resolution) of better than 0.5 microns (FWHM at 635 nm wavelength). The software system displayed changes in the z-axis with a precision of 0.1 micron. The tissue samples remained mounted on a single glass slide (as

used during the optical testing). The glass slide was placed on the instrument and measurements were attempted.

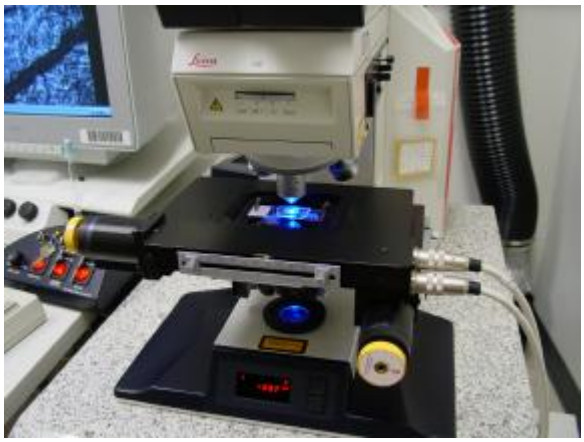

Figure 23. Close-up view of confocal microscope.

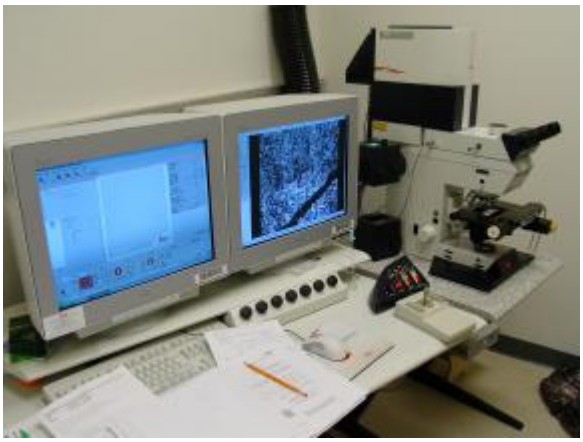

Figure 24. Dual screen setup for confocal microscope.

Using the microscope, it was possible to image the tissue via direct viewing through the eyepieces, or through computer imaging via photomultiplier tubes (PMTs). In order to determine the best method to measure the thickness of the tissue, different techniques were attempted. These included: acquisition of a spatial image stack using the PMTs, differential focusing through the tissue, and differential focusing from a mark on the slide to the tissue. In addition, some of these methods were repeated at two magnifications, and with and without the PMTs. One final method involved labeling the tissue with a phosphate solution. The results of these techniques are discussed in Section 5.

3.3.2.2 Atomic Force Microscope (AFM) Method

An atomic force microscope (AFM) (Molecular Imaging, Inc., model PicoSPM) was used to image the surface of the tissue. The AFM works by detecting the deflection of a cantilevered probe with a sharp microscopic tip. The tip is placed in contact with the surface measured and is scanned in an x-y pattern to cover the area of interest. The topology of the surface can this be captured with this system. For the AFM, the sample was mounted such that the edge of the tissue was near the probe. The probe was scanned in an attempt to detect the edge of the tissue and determine the height of the probe, as it transitioned from touching the glass slide surface to the tissue surface.

4. Review of Monte Carlo (2-D Diffusion) Modeling

An Adding-Doubling Method Model was used to analyze data from the irradiation of porcine tissues collected from this project. Analysis of data from initial porcine skin samples from early in the project did not give consistent results since the data was not consistent (especially, monochromator data).

A separate, smaller, parallel effort was completed looking at 2-D Monte Carlo Transport (MCT) modeling for infrared radiation transport through tissues. Due to expected azimuthal symmetry, results are applicable for analyzing actual (3-D) laboratory measurements.

4.1 Rationale for a 2-D Diffusion Model

The Transport Equation also known as the Boltzmann Equation from statistical mechanics is the starting point for modeling transport of any kind transport phenomena (e.g., radiation, neutrons, or other particles). For modeling radiation the Boltzmann Equation becomes an integro-differential equation known as the Transport Equation of Radiative Transfer. Diffusion theory, when applicable, is often used in order to allow simpler solutions and intuitive understanding of the processes compared to directly solving the Transport Equation of Radiative Transfer. In tissue and many other media the probability of scattering is much higher than the probability of absorption. This can be written as:

$$\mu_a << \mu_s(1-g).$$

where μ_a is the absorption attenuation coefficient in tissue, μ_s is the scattering coefficient and g is the mean cosine of the scattering angle.

When the diffusion approximation is valid, the scattering predominates over absorption and the transport equation can be solved in terms of spherical harmonics or Legendre Polynomials. When the zeroth and first moments of the multi-moment expansion of the transport equation for the radiance is used and higher order moments are thrown out, it is called the diffusion approximation.

The diffusion approximation is excellent for ocular tissue and is still valid in skin tissue where absorption is significant but far from dominant. There are many paper and publications on the application of Monte Carlo methods for photon and neutron transport. In the past decade there have been a growing number of researchers working specifically in the area of the transport of infrared photons through tissue.

MCNP is the largest Monte Carlo transport modeling user group with hundreds of modules written over the past 25 years. Many of these modules are available but only a few can be used for modeling infrared photon transport through tissue. The energy-dependent, probability distributions (microscopic cross-sections) for scattering and absorption, necessary for MCT modeling of skin and corneal tissues is not complete. It is expected that since the cornea shows more uniformity than skin tissue, that spatially lumped, energy-dependent, microscopic cross-sections should be more accurate for corneas. The primary focus of our review was on determining the availability (existence) of energy-dependent, probability distributions for scattering, necessary for MCT modeling of skin and corneal tissues. An assessment of literature and users of MCT packages showed that additional measurements, equipment, procedures, and analyses are necessary for the implementation of a 2-D MCT. A proposal for the development of 2-D MCT modeling was sent to AFRL by FIU based upon information obtained during this project and from former colleagues at the University of Michigan's Nuclear Engineering

Department, renown for its development of many Monte Carlo models and techniques. The proposal to AFRL included an estimation of the cost of a small research project to obtain the relevant microscopic cross-sections necessary for very accurate Monte Carlo modeling for a variety of tissue types.

5. Results

In this section we discuss the results obtained for the testing methods and measurements done for this project. Where results are listed for multiple tissue samples under the same test conditions, a mean value was calculated along with a standard error to derive a single number that was descriptive of the results for several tissue samples.

5.1 Monochromator

Using the monochromator setup, several cases were run to determine that the setup was working correctly. However, in all occasions, it was not possible to generate useful data, since at least one sensor would produce values that were within the noise threshold of the detector. In order to improve the illumination, a 250 W infrared bulb (incandescent) was tested, and a 600 W quartz-tungsten halogen bulb was also tested. The 250W bulb also produced values at or near the noise range of the sensor. The 600 W bulb, while producing more energy, was not able to produce significantly improved results. This bulb had a much larger (coil) filament. The larger filament resulted in an image that was larger than the tissue size (and the detector size). Therefore, the additional energy was removed by the diaphragms and was not useful in increasing the signal strength. In fact, results were comparable with the 600 W bulb and the 100 W quartz-tungsten bulb, which had a compact closely-packed ("dense") filament. For comparison, we note that the filament of the 100 W bulb measured 4.2 x 2.3 mm, whereas the filament for the 600 W lamp measured 4.0 x 13.5 mm.

The difficulties in using the monochromator were unfortunate, since this method would have allowed testing of any wavelength (within the 1-2 micron range). Moreover, with the monochromator setup, there would be less safety concerns when compared to the use of invisible lasers (although at 600 W, eye and skin protection were required due to the strength of the UV component of the broadband source). The main problem with this method was obtaining sufficient throughput from the monochromator illumination source. A possible way to overcome this limitation in the future would be to use appropriate condenser lenses (transparent to NIR) that would focus the filament to a smaller spot size.

5.2 Lasers

Using lasers, it was possible to collect useful data for the different tissue samples. The samples were numerical labeled from 1 to 34. Descriptions of the samples are found in Table 3.

Table 3. Sample descriptions.

Set #	Sample Numbers	Description
1	1-11	~20 micron thick skin samples
2	12-22	~10 micron thick skin samples
3	23-28	~0.75 mm thick skin samples with outer skin layer (dark)
4	29-34	~0.75 mm thick skin samples with deeper skin layer (white)

From these sets, some samples were rejected for being too small relative to the tissue holder aperture. The rejected samples were #14, 17, 19, and 20, which resulted in a total of 30 samples

tested. Due to the number of samples/laser test combinations, testing was performed over a period of several days. The data was collected in 6 sessions on different days as shown in Table 4. Note that tests on the 8th day were done to consider the effect of testing after an extended period of time. Due to a number of circumstances related to an active hurricane season, it was not possible to test the samples while "fresh" (within 24 hours post-mortem). Rather, the first day of testing did not occur until 7 days post-mortem.

Table 4. Test schedule.

Test day	Samples	Laser	Comments
1	1-5, 7,8	1313 nm	Sample 6 was inadvertently missed
2	2, 6, 9-13, 15, 16, 18, 21, 22	1313 nm	Sample 2 was repeated Sample 6 was tested
4	23-34	1313 nm	
5	1-13, 15, 16, 18, 21, 22	1064 nm	Samples 14, 17, 19, 20 were too small
6	23-34	1064 nm	
8	1, 8, 10, 16, 18, 21, 22	1313 nm, 1064 nm	Retesting of selected "good" samples

5.2.1 Laser (1064 nm wavelength)

Using the 1064 nm wavelength laser, noise and experimental data were collected for all three sensors, along with beam intensity measurements. The raw data from these measurements were processed to provide two values for each data file (the mean value and the standard error). The data showing mean values and errors are tabulated in Appendix B. Using the data in Appendix B, and Equations 3-1 to 3-3, the diffuse reflectance, diffuse transmittance and collimated transmittance were calculated for the various cases. In addition, the IAD method was used to calculate values for the albedo (a), the optical depth (τ), and the anisotropy coefficient (g). Using Equations 3-4 and 3-5, along with the thickness values for the tissue, the absorption and scattering coefficients were calculated and tabulated (see Tables 5-8). The thickness values used for the thin tissue are the nominal cutting values of the microtome. Visible and thermal images of the thin tissue samples (before testing) are shown in Figures 25 and 26. Figure 25 shows that while the background cardboard is at a cooler temperature than the surroundings (22.5° C), the samples themselves are nearly at the same temperature as the background room temperature of 24.8° C. During testing, the sample holder was 1° C warmer than the tissue due to the constant handling of the holder. Table 5 has a list of computed values based on experimental data taken for the 20-micron samples with the 1064 nm laser. Looking at R_d, the values are fairly consistent except for sample 3, where the value is significantly lower than for the other cases. The parameter with the most change was the collimated transmittance. This value had up to a factor of five difference in value. All of the samples were tested on the same day. The resulting scattering coefficient was 2200 ± 100 cm^{-1}, the absorption coefficient was 210 ± 20 cm^{-1}, and the anisotropy was 0.93. We note that the error values do not include the uncertainty in the thickness measurements (which could be up to 50%).

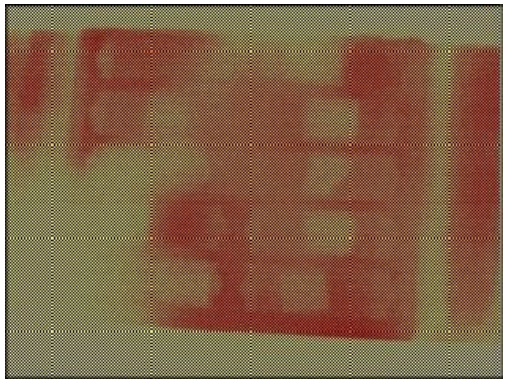

Figure 25. Thermal image of tissue before testing.

Figure 26. Visible image of thin tissue samples.

Table 6 has a list of computed values based on experimental data taken for the 10-micron samples with the 1064 nm laser. The values for R_d, and T_d, are very similar to those for the 20-micron tissue. The values for T_c and T_d, are slightly higher. Nevertheless, the values for the absorption and scattering coefficients are nearly twice those of the 20-micron samples. This casts doubt on the actual thickness of the 10-micron samples vs the 20-micron samples, since the factor of two difference could be explained if the actual sample thickness were nearer to 20 microns than to 10 microns. Measurements with the confocal microscope indicate that this might be a possibility (see Section 5.3.2.1). Comparison of Tables 5 and 6 also show that the calculated albedo, optical depth and anisotropy factor for all of the thin tissues were similar.

Table 7 has a list of computed values based on experimental data taken for the thick samples (epidermis) with the 1064 nm laser. The thickness values were obtained from the micrometer measurements in Table 20. The values for R_d are greater than those for the 20-micron samples, and T_d, is also very similar. The values for T_c are much lower, (as they should be) for the thicker tissue. The values for the absorption and scattering coefficients are 3.2 ± 0.3 $cm^{-1}$and 116 ± 10 cm^{-1}, while the anisotropy was 0.95. These values are significantly different from those calculated in Tables 5 and 6. Moreover, they do not include errors due to the possible change in thickness from the time of the experiment to the time of the measurement, which could cause an estimated 30% change in value.

Table 8 has a list of computed values based on experimental data taken for the thick samples that only include the dermis with the 1064 nm laser. The values for the absorption and scattering coefficients are 2.0 ± 0.1 cm^{-1} and 88 ± 3 cm^{-1}. Comparison of Tables 7 and 8 show similar values for the albedos, optical depths and anisotropy factors. However, the optical depth, τ, was significantly different for the thin and the thick tissues.

Table 5. Results 1064 nm laser, 20 micron tissue.

Experimentally-determined values				Values determined using IAD					
No.	R_d	T_d	T_c	a	τ	g	z (mm)	μ_s (cm^{-1})	μ_a (cm^{-1})
S1	0.070	0.496	4.80E-03	0.944	5.215	0.947	0.020	2500	150
S2	0.067	0.474	7.83E-03	0.930	4.726	0.939	0.020	2200	160
S3	0.038	0.326	6.60E-03	0.837	4.898	0.962	0.020	2100	400
S4	0.065	0.474	3.40E-03	0.939	5.560	0.951	0.020	2600	170
S5	0.060	0.304	6.65E-03	0.884	4.890	0.899	0.020	2200	280
S6	0.067	0.397	1.06E-02	0.907	4.423	0.912	0.020	2000	210
S7	0.062	0.374	5.30E-03	0.910	5.117	0.924	0.020	2300	230
S8	0.071	0.478	2.13E-03	0.949	6.030	0.951	0.020	2900	150
S9	0.062	0.355	7.76E-03	0.898	4.735	0.911	0.020	2100	240
S10	0.068	0.425	2.67E-02	0.893	3.500	0.896	0.020	1600	190
S11	0.068	0.436	8.18E-03	0.923	4.683	0.928	0.020	220	180
Mean	0.063	0.41	0.008	0.91	4.9	0.93		2200	210
Std Err ±	0.003	0.02	0.002	0.01	0.2	0.01		100	20

Table 6. Results 1064 nm laser, 10 micron tissue.

Experimentally-determined values				Values determined using IAD					
No.	R_d	T_d	T_c	a	τ	g	z (mm)	μ_s (cm^{-1})	μ_a (cm^{-1})
S12	0.069	0.422	1.28E-02	0.913	4.238	0.913	0.010	3900	371
S13	0.067	0.417	1.19E-02	0.910	4.307	0.916	0.010	3900	388
S15	0.062	0.413	1.17E-02	0.903	4.329	0.923	0.010	3900	419
S16	0.066	0.489	1.13E-02	0.927	4.364	0.939	0.010	4000	320
S18	0.068	0.424	3.94E-03	0.931	5.413	0.935	0.010	5000	374
S21	0.067	0.340	8.21E-03	0.898	4.679	0.897	0.010	4200	475
S22	0.066	0.335	1.47E-02	0.880	4.096	0.879	0.010	3600	490
Mean	0.066	0.41	1.1E-02	0.91	4.5	0.91	0.010	4100	410
Std Err ±	0.001	0.02	1E-03	0.01	0.2	0.01		200	20

Table 7. Results 1064 nm laser, thick tissue (dark).

Experimentally-determined values				Values determined using IAD					
No.	R_d	T_d	T_c	a	τ	g	z (mm)	μ_s (cm^{-1})	μ_a (cm^{-1})
S23	0.118	0.408	2.00E-05	0.974	10.8	0.943	0.89	120	3.1
S24	0.122	0.394	2.00E-05	0.974	10.7	0.938	0.87	120	3.2
S25	0.108	0.408	2.00E-05	0.972	10.7	0.946	1.24	80	2.4
S26	0.110	0.393	2.00E-05	0.971	10.8	0.943	1.17	90	2.6
S27	0.094	0.479	4.00E-05	0.973	10.2	0.959	0.71	140	3.9
S28	0.090	0.490	3.00E-05	0.973	10.2	0.962	0.68	150	4.1
Mean	0.107	0.43	2.5E-05	0.9728	10.6	0.948	0.93	120	3.2
Std Err ±	0.005	0.02	3.E-06	0.0004	0.1	0.004	0.09	10	0.3

Table 8. Results 1064 nm laser, thick tissue (light).

Experimentally-determined values				Values determined using IAD					
No.	R_d	T_d	T_c	a	τ	g	z (mm)	μ_s (cm^{-1})	μ_a (cm^{-1})
S29	0.100	0.560	5.00E-05	0.979	9.820	0.965	0.96	100	2.1
S30	0.060	0.690	1.80E-04	0.977	8.544	0.986	0.93	90	2.1
S31	0.086	0.609	7.00E-05	0.980	9.482	0.973	1.02	91	1.9
1S132	0.082	0.631	7.00E-05	0.981	9.543	0.976	1.13	83	1.6
S323	0.070	0.657	1.00E-04	0.979	9.189	0.981	1.13	80	1.7
S33	0.062	0.622	1.20E-04	0.973	8.955	0.981	1.09	80	2.3
S34	0.059	0.713	3.70E-04	0.977	7.854	0.987	0.78	98	2.3
Mean	0.074	0.64	1.4E-04	0.978	9.1	0.979	0.98	89	2.0
Std Err ±	0.006	0.02	4.E-05	0.001	0.3	0.003	0.05	3	0.1

To compare the test results with the literature, all of the results for the 1064 nm laser along, with published data are summarized in Table 9. Various sources [33, 34] cite an absorption coefficient for water near 1064 nm at values between 0.14 and 0.15 cm^{-1}. Moreover, tests have been performed on porcine dermis and human skin at these wavelengths. Du et. al. [32] published a graph with absorption and scattering coefficients for porcine skin dermis. Based on the graphs, values are estimated as: an absorption coefficient of 0.8 cm^{-1}, a scattering coefficient of 220 cm^{-1}, and anisotropy of 0.88, for samples ~ 30 hours post-mortem. In addition, Troy et. al. [35], obtained absorption and isotropic scattering coefficients for human skin in the near infrared wavelengths. They also provide a graph from which we can estimate the absorption coefficient as between 0.5 and 2 cm^{-1}. The isotropic scattering coefficient is approximately 12 cm^{-1} that, with anisotropy of 0.9, results in a scattering coefficient of 120 cm^{-1}.

Table 9. Comparison of 1064 nm results.

μ_s (cm^{-1})	μ_a (cm^{-1})	g	Material	Source
N/A	0.14-0.15		Water	[33, 34]
220	0.8	0.88	Porcine dermis	[32]
120	0.5-2	0.9	Human dermis	[35]
2200	210	0.93	Porcine epidermis	Project, 20 micron tissue
4100	410	0.91	Porcine epidermis	Project, 10 micron tissue
120	3.2	0.95	**Porcine epidermis and dermis**	Project, dark thick tissue
89	2.0	0.98	Porcine dermis	Project, light thick tissue

While performing the tests, it was noticed that the value of the collimated transmittance varied if the sample holder was rotated in the integrating sphere. In some cases, the changes were significant. For example, Table 10 shows the mean value for the collimated transmittance that was used for the calculations in Tables 5 and 6, along with the mean value when the sample was rotated 360 degrees. The ratio of the two values is shown in another column.

Table 10. Table showing difference in T_c when the sample was rotated.

Sample	T_c	Mean T_c over 360°	Ratio
S1	0.0048	0.0022	0.46
S2	0.0078	0.0234	2.99
S3	0.0066	0.0077	1.16
S4	0.0034	0.0050	1.46
S5	0.0067	0.0070	1.05
S6	0.0106	0.0353	3.33
S7	0.0053	0.0062	1.17
S8	0.0021	0.0022	1.05
S9	0.0078	0.0060	0.77
S10	0.0267	0.0233	0.87
S11	0.0082	0.0077	0.94
S12	0.0128	0.0136	1.06
S13	0.0119	0.0092	0.77
S15	0.0116	0.0088	0.75
S16	0.0113	0.0156	1.38
S18	0.0039	0.0040	1.02
S21	0.0082	0.0085	1.03
S22	0.0147	0.0106	0.72

To show the variation in the sensor reading when rotating the tissue holder, we also plotted all of the raw sensor readings for the T_c sensor (noting that T_c is directly proportional to the sensor readings), in Figure 27. The plot shows a variation of up to an order of magnitude for some of the samples. This variation in the collimated transmittance can cause significant variations in the optical properties computed. In order to further explore the effect of rotating the tissue, one of

the samples was mounted and rotated, while data was taken from each of the three sensors. These graphs are shown in Figure 28. This figure shows that there is little variation in the diffuse reflectance and transmittance; however, there is significant variation in the collimated transmittance. Possible explanations for this variation could be variations in the sample thickness which, if coupled with a slightly off-center sample, could cause those variations. Another possibility would be that the tissue sample was slightly small or did not fill the sample holder in a small section, and rotation would have allowed more radiation to go through. While in some cases the sample was slightly small, this latter explanation seems less likely, since the smallest samples were eliminated. Moreover, the sample would have to be significantly off-center.

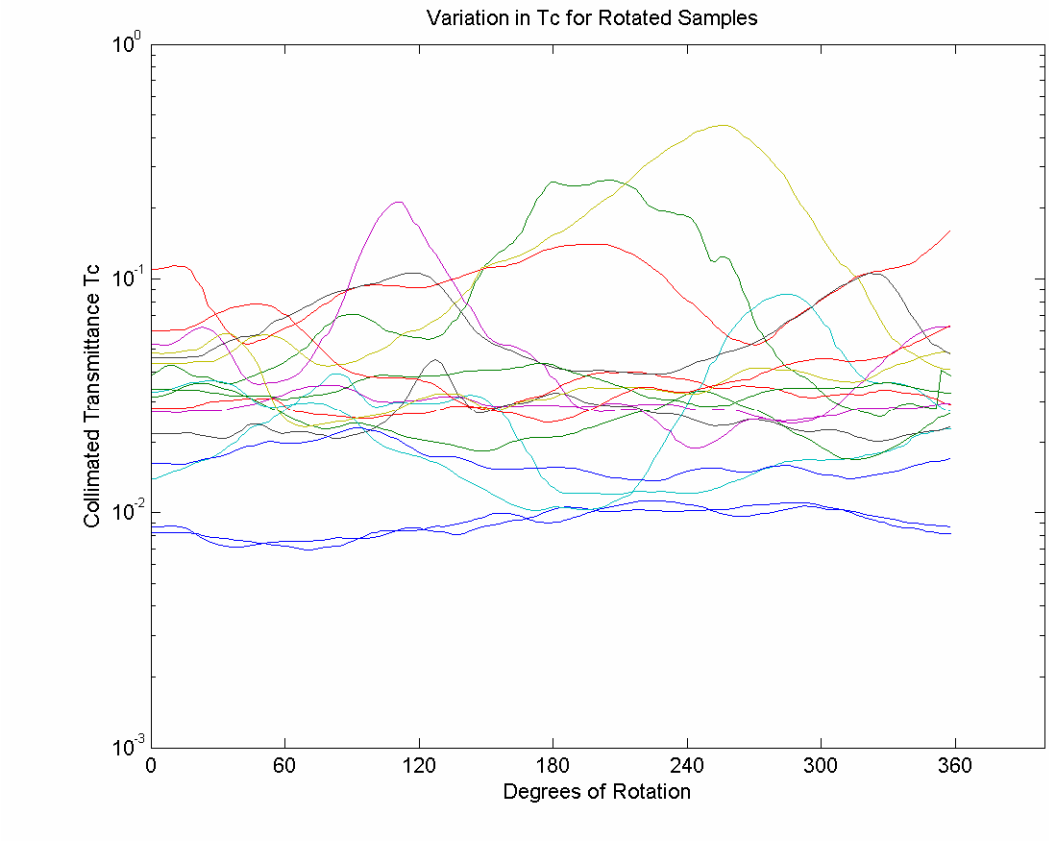

Figure 27. Collimated transmittance sensor reading while rotating sample.

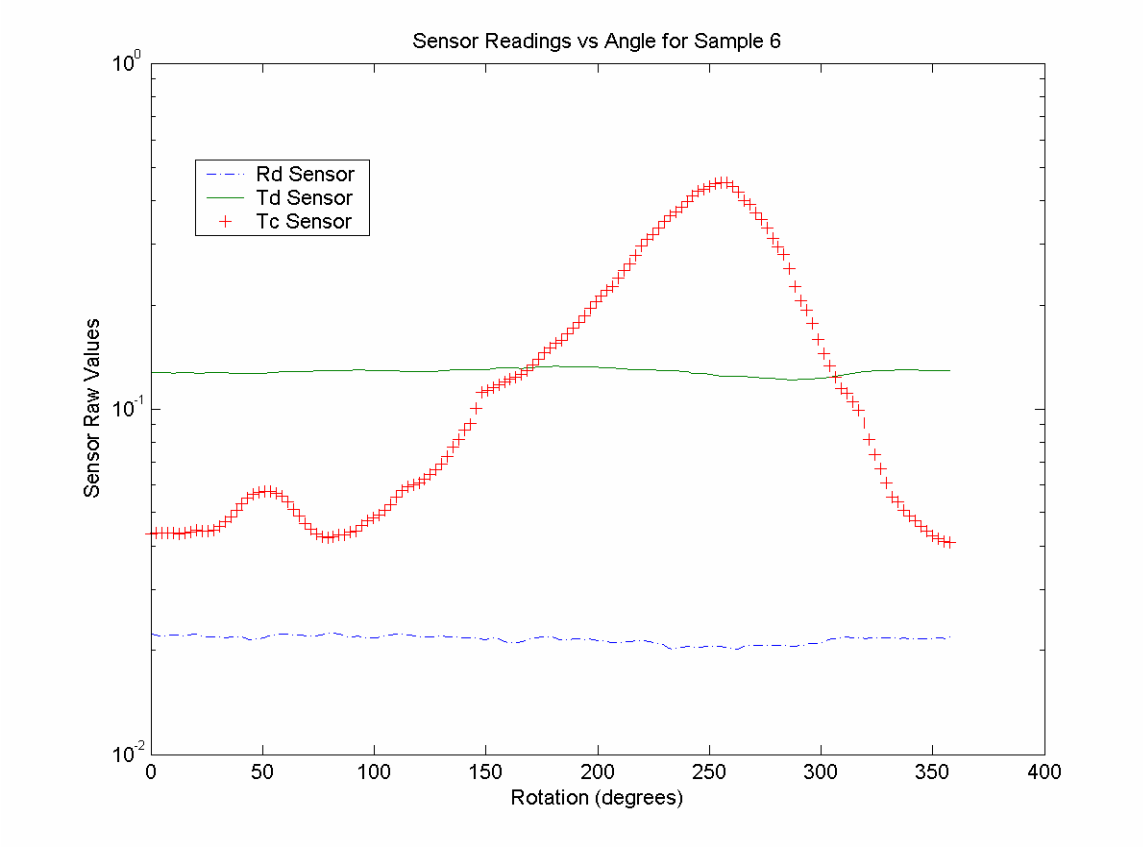

Figure 28. Raw sensor values when sample #6 was rotated.

5.2.2 Laser (1310 nm Wavelength)

Tables 11-14 show computed values for the optical properties of the tissue samples based on experimental values obtained with the 1313 nm laser. Table 11 shows the values for the 20-micron samples. The resulting scattering coefficient was 2000 ± 100 $cm^{-1}$and the absorption coefficient was 180 ± 30 cm^{-1}.

Table 12 shows values for the 10-micron samples with a scattering coefficient of 4100 ± 100 $cm^{-1}$and the absorption coefficient of 270 ± 20 cm^{-1}. Once again, these values are nearly double the values for the 20-micron samples and cast the same uncertainty over the tissue thickness. Tables 13 and 14 show results when using the thicker tissue. Table 13 is for tissue with the epidermis and Table 14 is for the tissue consisting of dermis. The scattering coefficient for the tissue with epidermis was 110 ± 7 cm^{-1} and the absorption coefficient was 4.6 ± 0.2 cm^{-1}. The scattering coefficient for the dermal tissue was 105 ± 5 cm^{-1} and the absorption coefficient was 2.8 ± 0.2 cm^{-1}.

Table 11. Results for 1313 nm laser, 20 micron samples.

Experimentally-determined values				Values determined using IAD					
No.	R_d	T_d	T_c	a	τ	g	z (mm)	μ_s (cm^{-1})	μ_a (cm^{-1})
S1	0.077	0.612	4.78E-03	0.966	5.220	0.963	0.020	2500	90
S2	0.049	0.467	3.51E-02	0.860	3.227	0.943	0.020	1400	230
S2-2	0.079	0.591	6.17E-03	0.963	4.965	0.956	0.020	2400	90
S3	0.051	0.358	6.88E-03	0.884	4.856	0.933	0.020	2100	280
S4	0.066	0.466	9.94E-03	0.924	4.488	0.935	0.020	2100	170
S5	0.038	0.303	1.69E-02	0.792	3.955	0.937	0.020	1600	410
S6-2	0.096	0.583	1.04E-02	0.965	4.439	0.937	0.020	2100	80
S7	0.060	0.418	1.87E-02	0.890	3.854	0.916	0.020	1700	210
S9	0.068	0.433	7.84E-03	0.922	4.725	0.928	0.020	2200	180
S10	0.084	0.503	2.40E-02	0.932	3.607	0.907	0.020	1700	120
S10-2	0.069	0.426	1.40E-02	0.911	4.143	0.912	0.020	1900	180
S11	0.080	0.475	8.36E-03	0.940	4.661	0.926	0.020	2200	140
Mean	0.068	0.47	.014	0.91	4.3	0.933	0.020	2000	180
Std Err ±	0.005	0.03	.003	0.01	0.2	0.005		100	30

Table 12. Results for 1313 nm laser, 10 micron samples.

Experimentally-determined values				Values determined using IAD					
No.	R_d	T_d	T_c	a	τ	g	z (mm)	μ_s (cm^{-1})	μ_a (cm^{-1})
S12	0.083	0.520	1.52E-02	0.943	4.065	0.924	0.010	3800	230
S13	0.085	0.551	6.87E-03	0.959	4.857	0.943	0.010	4700	200
S15	0.074	0.431	1.06E-02	0.922	4.426	0.914	0.010	4100	340
S16	0.079	0.510	1.34E-02	0.940	4.189	0.928	0.010	3900	250
S18	0.084	0.511	6.75E-03	0.951	4.875	0.935	0.010	4600	240
S21	0.084	0.436	1.37E-02	0.927	4.167	0.899	0.010	3900	300
S22	0.078	0.469	1.17E-02	0.933	4.324	0.920	0.010	4000	290
Mean	0.081	0.49	1.1E-02	0.939	4.4	0.923	0.010	4100	270
Std Err ±	0.002	0.02	1.E-03	0.005	0.1	0.005		100	20

Table 13. Results for 1313 nm laser, thick (dark) samples.

Experimentally-determined values				Values determined using IAD					
No.	R_d	T_d	T_c	a	τ	g	z (mm)	μ_s (cm^{-1})	μ_a (cm^{-1})
S23	0.092	0.255	3.00E-05	0.951	10.3	0.92	0.89	110	5.7
S23-2	0.102	0.288	3.00E-05	0.959	10.4	0.92	0.89	112	4.8
S23-W	0.250	0.095	3.00E-05	0.958	10.3	0.66	0.89	111	4.9
S23-W2	0.130	0.329	3.00E-05	0.969	10.3	0.92	0.89	113	3.6
S24	0.115	0.232	4.00E-05	0.954	10.1	0.89	0.87	111	5.3
S24-2	0.117	0.319	5.00E-05	0.963	9.8	0.92	0.87	108	4.1
S25	0.109	0.180	2.00E-05	0.947	10.6	0.88	1.24	81	4.5
S26	0.103	0.259	3.00E-05	0.955	10.2	0.91	1.17	83	3.9
S27	0.122	0.335	5.00E-05	0.967	9.9	0.92	0.71	135	4.7
S28	0.123	0.332	5.00E-05	0.966	9.9	0.92	0.68	141	4.9
Mean	0.126	0.26	3.6E-05	0.959	10.2	0.89	0.93	110	4.6
Std Err ±	0.016	0.03	4.E-06	0.003	0.1	0.03	0.09	7	0.2

Table 14. Results for 1313 nm laser, thick (light) samples.

Experimentally-determined values				Values determined using IAD					
No.	R_d	T_d	T_c	a	τ	g	z (mm)	μ_s (cm^{-1})	μ_a (cm^{-1})
S29	0.184	0.301	3.00E-05	0.975	10.52	0.88	0.96	107	2.7
S29-1	0.376	0.130	3.00E-05	0.977	10.52	0.58	0.96	107	2.5
S31	0.155	0.341	3.00E-05	0.974	10.37	0.91	0.93	109	2.9
S32	0.165	0.252	2.00E-05	0.968	10.58	0.87	1.02	100	3.3
S33	0.157	0.323	3.00E-05	0.973	10.32	0.90	1.13	89	2.5
S34	0.131	0.421	5.00E-05	0.975	9.87	0.94	1.09	88	2.3
S30	0.215	0.244	2.00E-05	0.974	10.56	0.84	0.78	132	3.5
Mean	0.20	0.29	3.0E-05	0.974	10.39	0.85	0.98	105	2.8
Std Err ±	0.03	0.03	3.E-06	0.001	0.08	0.04	0.04	5	0.2

To compare the test results with the literature, all of the results for the 1313 nm laser along, with published data are summarized in Table 15.

Various sources [33, 35, 36] cite an absorption coefficient for water near 1313 nm at values near 1.6 cm^{-1}. Moreover, tests have been performed on porcine dermis and human skin at these wavelengths. Du et. al. [32] published a graph with absorption and scattering coefficients for

porcine skin dermis. Based on the graphs, values are estimated as: an absorption coefficient of 1.2 cm^{-1}, a scattering coefficient of 220 cm^{-1}, and anisotropy of 0.88, for samples ~ 30 hours post-mortem. In addition, Troy, et. al. [35], obtained absorption and isotropic scattering coefficients for human skin in the near infrared wavelengths. They also provide a graph from which we can estimate the absorption coefficient of 2 cm^{-1}. The isotropic scattering coefficient is approximately 10 cm^{-1} that, with anisotropy of 0.9, results in a scattering coefficient of 100 cm^{-1}.

Table 15. Comparison of 1313 nm results.

μ_s (cm^{-1})	μ_a (cm^{-1})	g	Material	Source
N/A	1.6		Water	[33, 34, 36]
220	1.2	0.88	Porcine dermis	[32]
100	2	0.9	Human dermis	[35]
2000	180	0.93	Porcine epidermis	Project, 20 micron tissue
4100	270	0.92	Porcine epidermis	Project, 10 micron tissue
110	4.6	0.89	**Porcine epidermis and dermis**	Project, dark thick tissue
105	2.8	0.85	Porcine dermis	Project, light thick tissue

5.2.3 Age Testing

While not a part of the scope of the project, it was decided to retest some of the tissue samples several days after it was originally tested to compare the differences in values. Table 14 has the computed results when using the 1064 nm laser, while Table 15 has the computed results when using the 1313 nm laser. Comparing Table 14 with Tables 5 and 6, show that the older samples fell under the same range of values as in the prior tests.

Table 16. Retesting of thin tissue 3 days later (1064 nm laser).

Experimentally-determined values				Values determined using IAD					
No.	R_d	T_d	T_c	a	τ	g	z (mm)	μ_s (cm^{-1})	μ_a (cm^{-1})
S1	0.072	0.470	3.00E-03	0.945	5.686	0.945	0.020	2700	160
S8	0.071	0.475	2.51E-03	0.947	5.863	0.949	0.020	2800	160
S10	0.066	0.430	2.48E-02	0.895	3.573	0.902	0.020	1600	190
S16	0.065	0.477	3.16E-02	0.899	3.331	0.915	0.010	3000	340
S18	0.068	0.446	3.72E-03	0.936	5.470	0.941	0.010	5100	350
S21	0.068	0.365	9.04E-03	0.904	4.583	0.902	0.010	4100	440
S22	0.067	0.360	7.66E-03	0.905	4.748	0.905	0.010	4300	450

A comparison of Table 15 with Tables 10 and 11 show that while there were variations in the values, they were within the variation of the earlier tests.

Table 17. Retesting of thin tissue 7 days later (1313 nm laser).

Experimentally-determined values				Values determined using IAD					
No.	R_d	T_d	T_c	a	τ	g	z (mm)	μ_s (cm^{-1})	μ_a (cm^{-1})
S1-1	0.072	0.520	4.98E-03	0.949	5.179	0.950	0.020	2500	130
S8-1	0.063	0.438	1.59E-02	0.904	4.017	0.922	0.020	1800	190
S10-1	0.060	0.399	2.09E-02	0.881	3.746	0.906	0.020	1700	220
S16-1	0.058	0.462	9.52E-03	0.914	4.531	0.945	0.010	4100	390
S18-1	0.065	0.450	7.46E-03	0.925	4.775	0.936	0.010	4400	360
S21-1	0.065	0.488	1.62E-02	0.918	3.999	0.934	0.010	3700	330
S22-1	0.066	0.563	3.22E-02	0.924	3.311	0.940	0.010	3100	250

5.3 Tissue Thickness Measurement Results

As outlined in Section 3.0, several different methods were used to measure the thickness of tissue samples. When significant time elapsed between testing methods, one of the earlier methods was repeated for comparison purposes.

5.3.1 Thick Tissue Measurement Results

The thick tissues (~ 1 mm thick) were measured using a micrometer, an optical microscope system, and a laser profilometer. Samples labeled 23-28 were the top skin layer samples (dark samples), while samples 29-34 were the dermis samples (light samples). When these tests were performed, it was noted that the dark skin samples were relatively stiff, while the light samples were still soft and flexible.

5.3.1.1 Micrometer Measurement Results

The raw data from the thickness measurements, along with the calculated average values and standard errors are shown in Table 18. The tissue thickness is reported as the mean measured value minus the slide thickness. The values in Table 18 were obtained using the second method described in Section 3.3.1.1, where the micrometer was allowed to touch the slides but not compress them. This table shows that there is a factor of 2 variation between the minimum measured thickness and maximum measured thickness. This is due to the fact that the tissue samples were not fresh, and the dark samples tended to curl. This measuring method may not have compressed the sample sufficiently to flatten it out. This is particularly visible for samples #24 and 25. To compare this method with the first method wherein the micrometer was used as if measuring a rigid object (i.e., using the slipping of the thimble to control the applied force at the jaws), four of the tissue samples were measured again. These samples were #23, 25, 33, and 34. Table 19 shows the data collected, along with the mean value, the standard error, and the percent error using the values obtained from Table 16 as a baseline.

Table 18. Micrometer raw data and calculated tissue thickness values.

Sample No.	Measured values (3 times) (inches)			Calculated Mean (inches)	**Tissue Thickness (mm)**	**Std. Error ± (mm)**
Slides	0.0798	0.0798	0.0796	0.07973	0.00	0.002
23	0.1390	0.1182	0.1389	0.13203	1.3	0.2
24	0.1555	0.1582	0.1476	0.15377	1.88	0.08
25	0.1521	0.1693	0.1515	0.15763	2.0	0.2
26	0.1314	0.1470	0.1412	0.13987	1.5	0.1
27	0.1238	0.1308	0.1334	0.12933	1.26	0.07
28	0.1206	0.1174	0.1246	0.12087	1.04	0.05
29	0.1385	0.1413	0.1374	0.13907	1.51	0.03
30	0.1243	0.1303	0.1226	0.12573	1.17	0.06
31	0.1235	0.1306	0.1356	0.12990	1.27	0.09
32	0.1340	0.1292	0.1237	0.12897	1.25	0.08
33	0.1236	0.1428	0.1427	0.13637	1.4	0.2
34	0.1176	0.1197	0.1193	0.11887	0.99	0.02

Table 19. Comparison of micrometer measurement methods.

Sample No.	Three measured values when compressing the tissue (inches)			Calculated Mean (inches)	**Tissue Thickness (mm)**	**Std. Error ± (mm)**	**% Error relative to Table 16**
Slides	0.0798	0.0798	0.0796	0.0797	0.00	0.002	
B23	0.1163	0.1179	0.1120	0.1154	0.91	0.04	32
B25	0.1211	0.1193	0.1186	0.1197	1.01	0.02	49
B33	0.1164	0.1159	0.1157	0.1160	0.92	0.01	36
B34	0.1124	0.1110	0.1099	0.1111	0.80	0.02	20

Based on this table, it is clear that there is a significant difference (20%-49%) in measured tissue thickness when using the two different methods. In particular, we note that sample 25 was measured at nearly half the thickness using this method. Given the way our tissue was mounted, the method that did not compress the tissue would provide the most accurate results, assuming the tissue was not curled when it was measured. From these results, we reason that the best way of mounting the tissue to produce the most accurate thickness measurements would be to use a spacer that was slightly thinner than the tissue. Then, the tissue would be compressed between the slides until the spacer contacted the surfaces of the slide and stopped any further compression.

These micrometer thickness measurements were repeated 13 days later, after testing with the optical microscope, to be able to make an appropriate comparison between the optical method and the micrometer method. Results from the micrometer measurements taken 13 days later are shown in Table 20.

Table 20. Micrometer measurements repeated 13 days later.

Sample No.	Measured values (3 times) (inches)			Calculated Mean (inches)	**Tissue Thickness (mm)**	**Std. Error ± (mm)**
Slides	0.0800	0.0800	0.0798	0.0799	0.00	0.002
23	0.1172	0.1147	0.1128	0.1149	0.89	0.03
24	0.1155	0.1188	0.1085	0.1143	0.87	0.08
25	0.1260	0.1357	0.1242	0.1286	1.24	0.09
26	0.1319	0.1241	0.1224	0.1261	1.17	0.08
27	0.1088	0.1078	0.1070	0.1079	0.71	0.01
28	0.1048	0.1073	0.1086	0.1069	0.68	0.03
29	0.1156	0.1168	0.1205	0.1176	0.96	0.04
30	0.1193	0.1176	0.1131	0.1167	0.93	0.05
31	0.1177	0.1209	0.1211	0.1199	1.02	0.03
32	0.1252	0.1257	0.1223	0.1244	1.13	0.03
33	0.1238	0.1230	0.1220	0.1229	1.09	0.01
34	0.1092	0.1106	0.1116	0.1105	0.78	0.02

Table 21 shows a comparison of the data in Tables 18 and 20. Table 21 indicates that in the 13 days of storage, the thickness of the tissue decreased between 10 and 54% due to dehydration. In particular, the samples taken from the outer skin layer (dark samples 23-29) had a much greater tendency to dehydrate and curl than the samples from the dermal tissue layer (light samples 30-34).

Table 21. Comparison of thickness measurements after 13 days.

Sample No.	Thickness (From Table 16) (mm)	Thickness (From Table 18) (mm)	% Error
23	1.33	0.89	33
24	1.88	0.87	54
25	1.98	1.24	37
26	1.53	1.17	23
27	1.26	0.71	44
28	1.04	0.68	34
29	1.51	0.96	36
30	1.17	0.93	20
31	1.27	1.02	20
32	1.25	1.13	10
33	1.44	1.09	24
34	0.99	0.78	22

5.3.1.2 Laser Profilometer Measurement Results

The laser profilometer was used to test the ability of this system to measure the tissue thickness. In general, the laser profilometer had difficulties in reading values when surfaces of different albedos are scanned. Moreover, the system had more difficulties reading dark materials (due to

absorption of the laser and the resulting weakness of the reflected signal). When trying to read the thickness of the tissue with the epidermis (dark samples), the system was not able to give correct results. When the sample was placed in the field of the laser and removed, the system could not properly account for the difference in the surfaces with tissue and without tissue. Even when the dark sample was placed in a cardboard background of similar color, the laser profilometer was not able to provide correct results. However, moving the tissue up and down during measurement by the laser did provide correct trends. Thus, when the tissue was moved towards the sensor, the system recorded a decrease in distance between the sensor head and the tissue. Similarly, when the tissue was moved away form the sensor, the proper trend was observed. The problem occurred only when trying to measure the top surface of the tissue and a bottom reference surface. In contrast to the difficulties in reading the dark samples, the system was able to provide measurement values for the light samples (samples 29-34).

Data was collected using the laser profilometer on the light (dermis) samples. The system collected data at 40 Hz which, in the four second data collection period, resulted in 160 data points for each tissue measured. The first two seconds of data measured the distance to the surface on which the tissue was placed. This was the "bottom" measurement. The tissue was then suddenly moved so that the center was imaged by the profilometer for another two seconds, yielding the "top" measurement. At the moment of the switch from top to bottom measurement, there is some fluctuation in the data until it stabilized. The bottom measurement was determined by averaging samples for the first 1.5 seconds and the top measurement was determined by averaging the samples over the last 1.5 seconds (thus avoiding the measurement discontinuity at or about 2 seconds). The averaged top and bottom measurements were subtracted to obtain the tissue thickness.

Data was also collected for a reference surface, whose thickness was measured with the micrometer. The thickness of the reference surface was used to convert the voltage readings from the profilometer to distances in millimeters. For comparison, the tissue was measured using the micrometer and two glass slides as described in the previous section, since these measurements were made 23 days later relative to those in Table 18. The values from the micrometer readings are found in Table 22. The standard error for these measurements is limited by the slide measurement, which exhibited more variation than some of the tissue measurements.

Comparison of the micrometer values and the laser profilometer values are found in Table 23. As shown in Table 23, the laser profilometer was not able to accurately determine the thickness of the light-colored tissue. Therefore, this method is not recommended for measuring the tissue thickness for any of the samples.

One possible way that this method could be modified to produce good results is to place the tissue between two slides and add a reflective surface underneath the bottom slide and underneath the top slide. Then, the distance between these points could be determined with the profilometer, and the thickness of the bottom slide would be subtracted out. When using this method, care should be taken to ensure the slides remain parallel throughout the method.

Table 22. Micrometer readings 23 days later (for comparison with laser profilometer).

Sample#	Three measurements (in)			Calculated Mean (in)	**Tissue Thickness (mm)**	**Std. Err ± (mm)**
Slides	0.0800	0.0796	0.0810	0.0822	0.0000	0.001
29	0.1210	0.1208	0.1213	0.1210	0.9864	0.001
30	0.1216	0.1221	0.1233	0.1223	1.019	0.002
31	0.1260	0.1288	0.1284	0.1277	1.157	0.003
32	0.1231	0.1241	0.1230	0.1234	1.047	0.002
33	0.1184	0.1178	0.1181	0.1181	0.9119	0.001
34	0.1096	0.1100	0.1092	0.1096	0.6960	0.002

Table 23. Comparison of laser profilometer and micrometer readings.

Sample #	Laser Profilometer (mm)	Micrometer (mm)	% Error
29	0.6970	0.9864	-29
30	1.141	1.019	12
31	1.084	1.157	-6
32	0.7027	1.047	-33
33	1.647	0.9119	81
34	1.544	0.6960	122

5.3.1.3 Optical Microscope Measurement Results

The tissue samples were mounted as described in Section 3.3.1.3. Samples 23-28 were imaged using the two microscope slide method. The software was calibrated using a ruled reticle (see Figure 29). When this method was applied to samples 29-34, there was difficulty in accurately detecting the edge of the tissue. Therefore, samples 29-34 were imaged using the single microscope slide method. Data from the measurements are shown in Table 24.

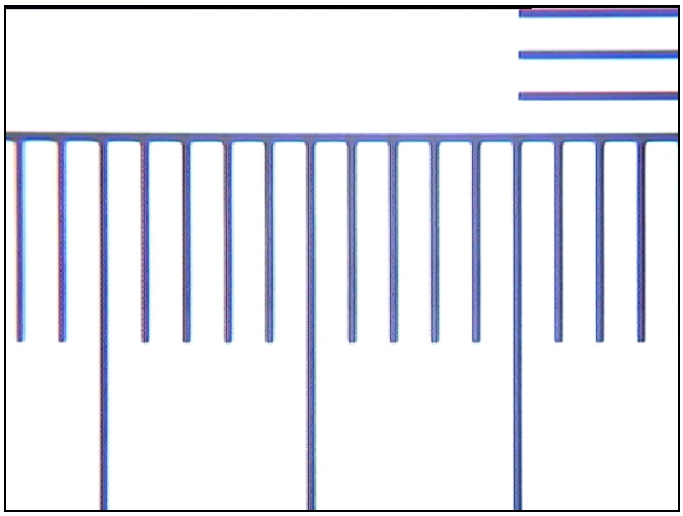

Figure 29. Calibration reticle as seen through microscope (0.1 mm/division).

Table 24. Optical microscope thickness measurements.

Sample #	Raw Measurements (mm)			**Thickness** (mm)	**Std. Error** ± (mm)
23	0.373	0.419	0.389	0.394	0.013
24	0.496	0.494	0.499	0.496	0.001
25	0.586	0.675	0.598	0.620	0.028
26	0.455	0.463	0.458	0.459	0.002
27	0.931	0.777	0.908	0.872	0.048
28	0.739	0.647	0.675	0.687	0.027
29	1.051	1.015	1.041	1.036	0.011
30	0.934	0.862	0.99	0.929	0.037
31	0.88	0.872	0.867	0.873	0.004
32	1.059	1.023	1.038	1.040	0.010
33	0.954	0.967	0.974	0.965	0.006
34	0.662	0.637	0.645	0.648	0.007

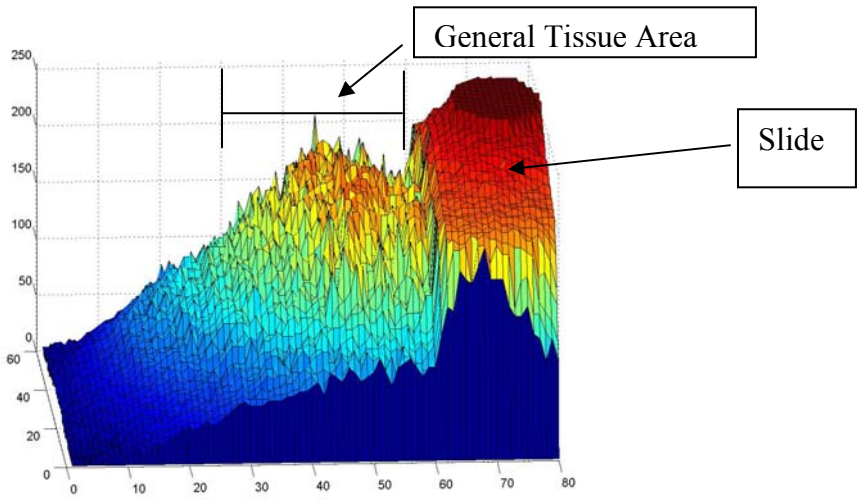

Figure 30. Image processing to attempt to determine tissue thickness.

When using this method, care must be taken, since the edge of the tissue may have slight thickness variations. When positioning the measuring lines with the software, thickness variations can be visually averaged, since the software generates a straight line that can be positioned at the average location of the edge of the tissue. When using this method, it was difficult to discern the edges of the dark tissue, and it was much easier to measure the light tissue. In order to improve the measurement of the tissue thickness, various image processing methods were attempted on the dark tissue. One of these methods was a three dimensional surface plot of pixel value (using the green plane of the RGB signal) at each x and y pixel locations. While this method could easily show the edge of the slide, the other edge of the tissue was difficult to find, since it slowly fades in brightness (see Figure 30). Another method attempted was to use an edge-detection algorithm (see Figure 31). This method was not successful in improving the results, due to the gradual change in pixel brightness. The raw image that was processed to produce Figures 30 and 31 is shown in Figure 32. A summary of all of the results for the thick tissue testing is found in Figure 33.

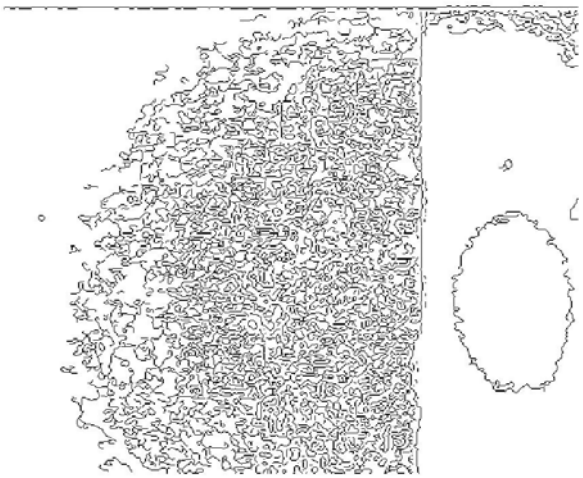

Figure 31. Edge detection to attempt to determine tissue thickness.

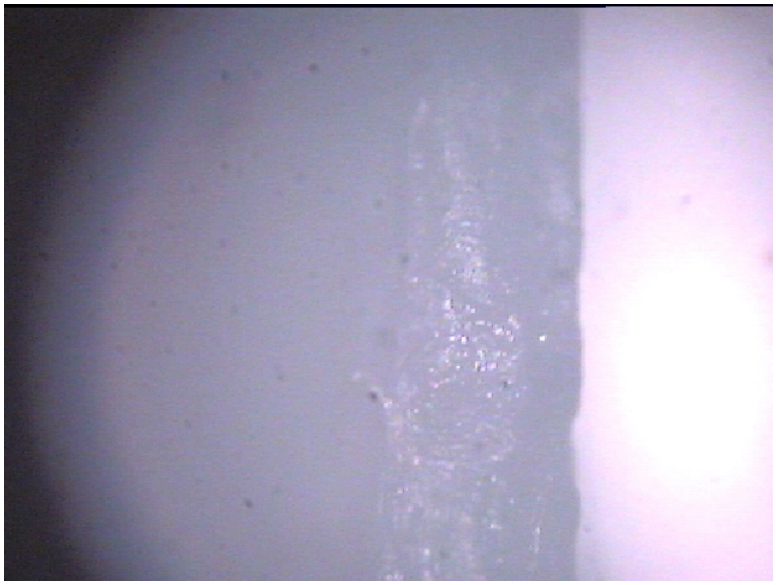

Figure 32. Raw image processed in Figures 30 and 31.

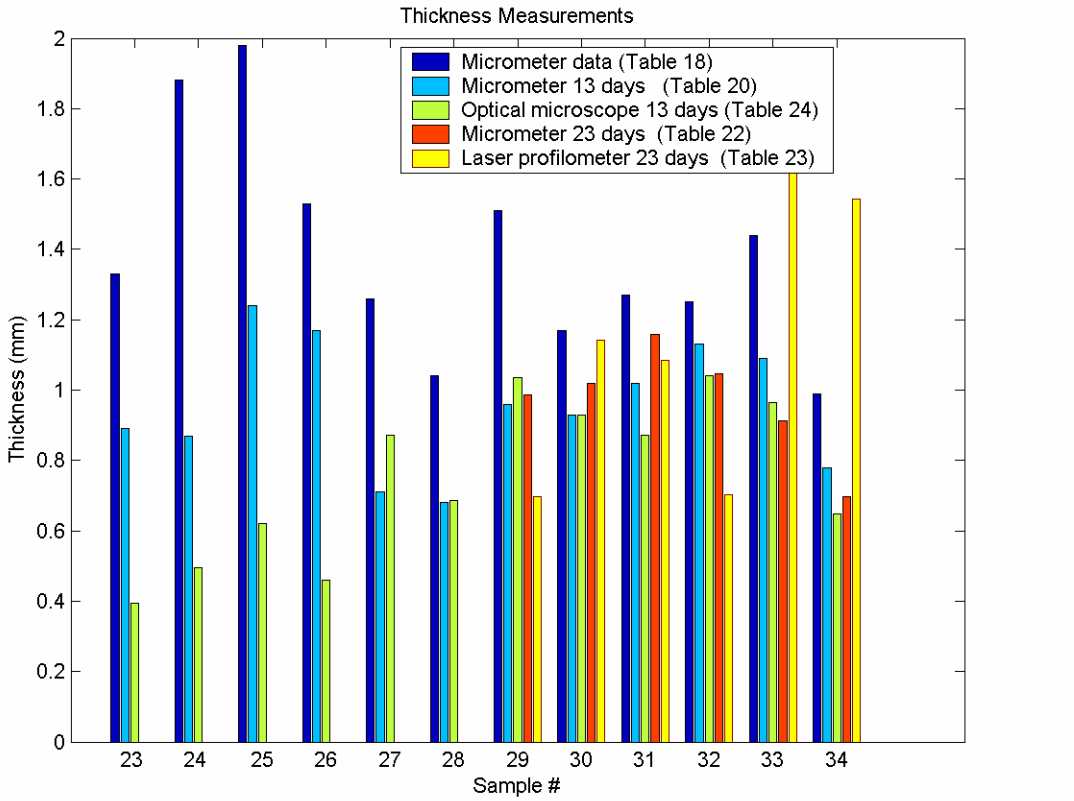

Figure 33. Comparison of all thickness measurements.

Figure 33 show that the optical microscope (with the light tissue) gave thickness measurements similar to the micrometer measurements. However, the optical microscope gave poor values with the dark tissue. This was mainly due to difficulties in discerning the edges of the tissue through the microscope. It also shows the large values obtained during the first micrometer measurements, where the samples were slightly curled and produced thicker values than the actual values.

Based on these results, the best method for measuring the tissue thickness is using the micrometer on the tissue sandwiched between two slides; however, as indicated above, it is necessary to use the proper technique to not compress the tissue. Given proper illumination of the sample, the optical microscope method is also a viable option. Finally, the laser profilometer is not recommended for measuring tissue thickness.

5.3.2 Thin Tissue Measurement Results

5.3.2.1 Confocal Microscope

Using the methods described in Section 3.3.2.1, several of the samples were used in an attempt to determine their thickness using a confocal microscope. The different methods were: use of the shallow depth of field of the confocal microscope to image the top and bottom surface of the tissue by adjusting the z (vertical) position of the microscope stage, the same method repeated but using a mark on the slide to determine the bottom of the tissue, and acquisition of a spatial image stack at various depths using the photomultiplier tubes (PMTs). In addition, some of these

methods were repeated at two magnifications, and with and without the PMTs. In all of these cases, the tissue was on a slide and no chemical additives were added. For a final test, a phosphate solution was used to image the tissue.

The first method was an attempt to view through the tissue, taking advantage of the extremely shallow depth of field designed in a confocal microscope. Attempts at visually seeing through the tissue were disappointing. It was not possible to image through the tissue in this fashion. Instead, the tissue was moved in search of anomalies such as small holes (from the animal's hair) or punctures in the tissue. Additionally, the tissue was imaged near the edge, where there would be a possibility of discerning tissue near the bottom of the sample due to irregular cutting near the edge. The idea was that such areas would allow for focusing along the side of the hole or edge of the tissue (assuming the side was visible). In some cases, it was possible to focus on the bottom of an indentation in the tissue, but it was unknown, how much distance remained between the bottom of the indentation (which still had some tissue), and the bottom of the slide. After many attempts, with low and high magnifications, the results were deemed unreliable. The holes in the tissue from the hair were fairly straight through the tissue and the sides of the hole were not readily visible through the microscope. Holes from other anomalies were also considered unreliable, since areas around the tears at times were thicker or thinner and not representative of the thickness of the tissue. It was also difficult to visually distinguish focusing changes for movement of the z-stage of up to 4 microns.

This method was also repeated using the PMTs to show an image of the tissue. The image was not of very high resolution, and was very grainy. Moreover, it was very difficult to judge when the image was focused at a given depth. Repeated attempts were not able to produce reproducible, reasonable numbers (numbers achieved were on the order of 100 microns thickness). Other attempts were to try to image the edge of the tissue. While these areas could provide sections that could be focused, the thickness of the edge of the tissue is not necessarily representative of the thickness of the rest of the tissue. This is due to the expected thinness of the tissue due to the microtome cutting operation.

The second method attempted to make up for the difficulty in imaging the bottom surface of the tissue by making an artificial mark on the slide, adjacent to the tissue. The mark was initially made with a magic marker. Using the confocal microscope, it was difficult to determine the best focus for the mark. When the mark was made, small ink droplets were splattered nearby. The image was deemed to be in focus when the small splattered ink droplets became visible. Even with this method, it was not possible to obtain reasonable, reproducible results. When using the PMTs, it was easy to see the ink mark in focus. However, it was difficult to determine the z-axis position of the mark, since adjustment in the z-axis did not show clear changes to the mark, unless the changes were greater than the expected thickness of the tissue. Had this method worked, there would have been a small error from the unknown thickness of the ink mark.

The third method used the PMTs and software to take images at various cross sections of the tissue and assembling them as a three-dimensional image. A limitation of this method is the z-axis movement which can only be increased at a fixed discrete step size based on the top slice z position, bottom slice z position, and the number of frames. Using this method near the edge of the tissue, it was easy to detect the bottom surface (face of the microscope slide), but it was difficult to determine the top surface of the tissue. The tissue showed many deep hills and valleys that were an order of magnitude above the expected tissue size.

Since there were difficulties in accurately determining the thickness of the tissue, several samples were processed to increase the possibility of obtaining a proper reading. These samples were labeled using two drops of a phosphate solution and covered with a cover slip. The cover slip was sealed using acetone along the periphery of the cover slip. One sample tested this way was a 5-micron sample. Measuring the thickness at different locations resulted in readings of 12.3, 11, 10.6, and 9.91 microns for an average of 11.0 ± 0.5. A 10-micron sample resulted in readings of 36, 25, 25.9, 27.1, and 32.4, for an average of 29 ± 2. A 20 micron sample was measured at four different locations producing values of 20.6, 18.8, 19.2, and 20.3 microns for an average of 19.7 ± 0.4 microns. These results indicate that this method worked well to measure the 20-micron sample. The discrepancies for the 5 and 10-micron sample can be due to an improper (non-reproducible) cutting technique with the microtome. These samples were taken early in the process of familiarization with the microtome. The microtome has a wheel for cutting that, if reversed, and then moved in the normal direction will result in a cut that is twice as thick. It is likely that the 5 micron sample was cut in this fashion and was actually a 10 micron sample, while the same thing may have occurred twice with the 10 micron sample producing a 30 micron sample.

5.3.2.2 Atomic Force Microscope

Using the methods described in Section 3.3.2.2 a tissue sample on a glass slide was placed in the atomic force microscope (AFM). One of the main limitations of the system was that it was time consuming to scan small areas of the tissue. Moreover, the scanned regions are fairly small. This necessitated trying to use the edge of the tissue to detect a step change in height. This method was not explored in full detail but rather, it was explored to determine whether it had potential for measuring the tissue thickness. Based on preliminary results, it appears that this method does have potential. While this method is a contacting method (where the AFM cantilever probe touches the sample), there was no visible adverse effect to the tissue.

This page intentionally left blank

6. Conclusions

A number of different test and measurement methodologies were tried in order to find improved ways of measuring the optical properties of biological tissue in the near infrared. In particular, three test setups were constructed to measure the reflectance, transmittance, and/or anisotropy factor of the tissue. Two of the setups utilized a double integrating sphere arrangement with a sensor in each sphere to measure diffuse reflectance and transmittance, along with a third sensor to measure collimated transmittance. The main difference between the setups was the illuminating source, where one of the setups used a monochromator and the other used lasers. When using the monochromator with a 100 W quartz-halogen bulb (or even a 600 W bulb) the signal values were within the noise threshold of the sensors. However, when using the lasers, it was possible to generate a signal beyond the noise level. Based on theoretical considerations, the setup for the anisotropy factor was not used, since it was believed that the samples would not be thin enough to result in single scattering of the radiation.

The measured reflectance and transmittance values were entered into an inverse adding-doubling model to calculate the optical properties of the tissue at 1064 nm and 1313 nm. The results for thin tissue were an order of magnitude above other published results; however, measurements with the thicker samples were similar to published results for human dermis. For the thick tissue, the scattering coefficient ranged between 80 and 150 cm^{-1} while the absorption coefficient ranged between 1.6 and 4.1 cm^{-1} when using the 1064 nm laser. For the 1313 nm laser, the scattering coefficient ranged between 81 and 141 cm^{-1}, while the absorption coefficient ranged between 2.5 and 5.7 cm^{-1}.

Since the tissue samples tested were of different thickness, several methods and methods were tried to accurately measure the thickness of the tissue. These methods included micrometer readings, optical microscopy, laser profilometry, confocal microscopy, and atomic force microscopy. For thick tissue, the micrometer readings were easy to make, accurate and repeatable. However, care must be taken when using the micrometer so to not compress the tissue. Optical microscopy (with the tissue on its side) also has potential as a good method for measuring the thickness. Limitations of this method include the difficulty in determining the edges of the tissue, particularly when the sides were not cut evenly, and the depth of field limitations which may not allow focusing of both sides simultaneously. Laser profilometry did not work at all on the dark tissue, although it did provide results for light tissue. Nevertheless, the readings for the light tissue were very inaccurate.

For thin tissue, the confocal microscope and the atomic force microscope have potential for measuring the tissue thickness. With these two methods, it is necessary to image the bottom and the top of the tissue. This can be done near an edge or a “hole” in the tissue. A clean, slanted cut (relative to the depth or z- direction) should allow the AFM probe to transition from the surface of the tissue to the slide or surface where the tissue is mounted. Moreover, it would allow the confocal microscope more opportunity to focus on the bottom and on the top of the tissue. A limitations of the confocal microscope used was that it was difficult to visually discern changes in tissue focus depth when the stage is moved by as much as four microns for an unprepared sample (an unprepared sample is one where the tissue is just mounted on a slide with no chemicals added). This can result in a 40% error in measurement for a 20 micron sample (4 microns for the top measurement and 4 microns for the bottom measurement). By using a phosphate-based solution, an experienced operator was able to accurately measure the thickness of a sample. A limitation of the atomic force microscope used was that it could only scan a very

small segment of the tissue. Thus it is necessary to make sure that the edge of the tissue was properly prepared and is representative of the thickness of the rest of the tissue. Nevertheless, the AFM showed potential for measuring the thickness of very thin tissue samples.

Due to the inability to get the monochromator to function with adequate signal strength, difficulty in cutting micron thin samples, and a detector malfunction, it was decided in conference call with contract officer from Northrop Grumman and AFRL chief scientists that FIU should concentrate entirely upon porcine tissues and not proceed with the rabbit cornea experiments as originally planned. In addition to the likely steep learning curve required for this new tissue, the modeling of the cornea is entirely different from that of skin tissue (much less scattering). We received a 2 micron laser from the AFRL on April 29, 2005 and returned it on May 25, 2005 (since it was needed back at Brooks AFB by June 1, 2005). We were unable to use this laser since it was a 20W Class IV laser. To use it would have required a beam attenuator to reduce the power several orders of magnitude. In addition, the Class IV laser would have required changing facilities to comply with the Health and Safety requirements of the university.

The objective of supporting Universities capabilities to measure transport coefficients in biological tissue was met by this research. FIU now has microtome, procedures, all equipment (except a couple high intensity infrared lasers) in order to carry out further experiments and collect, analyze and publish results for the absorption, transmission and scattering of infrared radiation at various IR wavelengths. It is also believe that a higher energy, yet small diameter IR source, identified as commercially available after the project's completion, would allow our current set of detectors to measure highly accurate, publishable data using this source and a monochromator instead of IR lasers.

7. References

1. Yoon, G., "Absorption and Scattering of Laser Light in Biological Media—Mathematical Modeling and Methods for Determining the Optical Properties," Ph.D. Dissertation, University of Texas-Austin, 1988.
2. Welch, A. and Van Gemert, M., Optical Thermal Response of Laser-Irradiated Tissue, Plenum Press, 1995.
3. Tortora, G. and Grabowski, S., Principles of Anatomy and Physiology, Harper Collins Publishers, 1996.
4. Vargas, G., Chan, E., Barton, J., Rylander, G., Welch, A., "Use of an Agent to Reduce Scattering in Skin," Lasers in Surgery and Medicine, 24, pp.133–141, 1999.
5. Niemz, Markolf, Laser-Tissue Interactions: Fundamentals and Applications, Third Revised Edition, Springer, Berlin, Germany, 1996.
6. Bohren, C. and Huffman, D., Absorption and Scattering of Light by Small Particles, Wiley Science Series, 1983.
7. Jenkins, F. and White, H., Fundamentals of Optics 4th Edition, McGraw-Hill Physics Series, 1981.
8. Jacques, S., "Origins of Tissue Optical Properties in the UV visible and NIR Regions," OSA TOPS on Advances in Optical Imaging and Photon Migration, 2, pp. 364-369, 1996.
9. Ishimaru, A., Wave Propagation and Scattering in Random Media—Single Scattering and Transport Theory Vol. 1, Academic Press, 1978.
10. Van Gemert, M., Jacques, S., Sterenborg, C., and Star, W., "Skin Optics," IEEE Transactions on Biomedical Engineering, v. 36, no. 12, pp. 1146-1154, 1989.
11. Hecht, E., Optics, 3rd Edition, Addison-Wesley Press, 1988.
12. Wilson, B., Jacques, S., "Optical Reflectance and Transmittance of Tissues: Principles and Applications," IEEE Journal of Quantum Electronics, v. 26, no. 12, December 1990.
13. Thody, A., Higgins, E., Wakamatsu, K., Ito, S., Burchill, S., and Marks, J., "Phoemelanin as Well as Eumelanin is Present in Human Dermis," Journal of Investigative Dermatology, v. 97, pp. 340-344, 1991.
14. Krishnaswamy, A., and Baronoski, G., "A Study on Skin Optics," Technical Report CS-2004-01, University of Waterloo, Waterloo, Canada, January 2004.
15. Jacques, S., and Prahl, S., "Modeling Optical and Thermal Distributions in Tissue During Laser Irradiation," Lasers in Surgery and Medicine, v. 6, pp. 494-503, 1987.
16. Tuchin, V., "Light Scattering Study of Tissues," Physics—Uspekhi, v. 40, no. 5, pp. 495-515, 1997.
17. Wan, S., Anderson, R., and Parrish, J., "Analytical Modeling for the Optical Properties of Skin with *In Vitro* and *In Vivo* Applications," Photochemistry and Photobiology, v. 34, pp. 493-499, 1981.
18. Cheong, W., Prahl, S., and Welch, A., "A Review of the Optical Properties of Biological Tissues," IEEE Journal of Quantum Electronics, v. 26, no. 12, pp. 2166-2185, 1990.
19. Wilson, B., Patterson, M., and Flock, S., "Indirect *versus* Direct Techniques for the Measurement of the Optical Properties of Tissues," Photochemistry and Photobiology, v. 46, no. 5, pp. 601-608, 1987.
20. Chandrasekhar, S., Radiative Transfer, Dover Press, 1960.
21. Wolbarsht, Myron L., "Laser Surgery: CO_2 or HF," IEEE Journal of Quantum Electronics, Vol. QE-20, No.12, pp. 1427-355, 1984.

22. Kubelka, P. and Munk, F. “Ein Beirag zur Optik der Farbanstriche,” Zeitsche. F. Techn. Physik, 11a:593-600 (1931)
23. Anderson, R., Parrish, J., “The Optics of Human Skin,” The Journal of Investigative Dermatology, v. 77, pp. 13-19, 1981.
24. Prahl, S., van Gemert, M., Welch, A. “Determining the optical properties of turbid media by using the adding doubling method,” Applied Optics, v. 32, no. 4, pp. 559-568, 1993.
25. Prahl, S., “Determining the optical properties of turbid media using the adding-doubling method” Applied Optics. 32, 559-568, 1993.
26. Prahl, S., “Optical Property Measurements Using the Inverse Adding Doubling Method” Oregon Medical Laser Center, St. Vincent Hospital, 1995.
27. http://omlc.ogi.edu/calc/iad_calc.html
28. Pickering, J., Prahl, S., Wieringen, N., and Beek, J., “Double Integrating Sphere System for Measuring the Optical Properties of Tissue,” Applied Optics, v. 32, no. 4, pp.399-410, 1993.
29. Vesselina, T. and Stoykova, E., “Refractive index measurement in human tissue samples,” 2000.
30. Dehghani, H. and Brooksby, B., “The effects of internal refractive index variation in near-infrared optical tomography: a finite element modeling approach,” Phys. Med. Biol., 48, 2713-2727, 2003.
31. www.laser-ndt.com/LP_method.html
32. Du, Y., et. al., “Optical properties of porcine skin dermis between 900nm and 1500nm,” Phys. Med. Biol., 46, 167-181, 2001.
33. Kou, L. and Labrie, D., and Chylek, P., "Refractive indices of water and ice in the 0.652.5μm spectral range," Appl. Opt., 32, 3531--3540, 1993.
34. Segelstein, D.J., "The complex refractive index of water," University of Missouri-Kansas City, 1981.
35. Troy, T. and Thennadil, S., “Optical Properties of Human Skin in the Near Infrared Wavelength Range of 1000 to 2200 nm,” Journal of Biomedical Optics, Vol. 6, No. 2, pp. 167-176, April 2001.
36. Wieliczka, D. M., Weng, S., and Querry, M. R., "Wedge shaped cell for highly absorbent liquids: infrared optical constants of water," Appl. Opt., 28, pp. 1714-1719, 1989.

Appendix A: Basic program for Merlin lock-in amplifier interface to computer

```
' MERLIN.BAS program listing:

' PROGRAM FOR DATA ACQUISITION FROM MERLIN
' AND TO SAVE DATA TO A DATA ARRAY AND TO A DISK FILE

Progloop:

CLEAR
OPTION BASE 0
INPUT "Enter output file name "; nam$
PRINT "Waiting"
z = TIMER
WHILE TIMER - z < 10
WEND
BEEP
PRINT "Sampling"
Number% = 100
OPEN "COM1:9600,N,8,1" FOR RANDOM AS #1

OPEN nam$ + ".txt" FOR OUTPUT AS #2
DIM a AS STRING * 17
PRINT " MERLIN DATA:"
z = TIMER
minrslt = 10
WHILE TIMER - z < 30

count = count + 1
         PRINT #1, "PR 0 /R"
         GET #1, 2, a
         PRINT #1, "TD1 3 /R"
         GET #1, , a
         IF MID$(a, 7, 1) = "0" THEN Sign$ = "+" ELSE Esing$ = "-"
         IF MID$(a, 8, 1) = "0" THEN Esing$ = "+" ELSE Esing$ = "-"
         Exp$ = Esing$ + MID$(a, 9, 2)
         Man$ = Sign$ + MID$(a, 12, 1) + "." + MID$(a, 13, 3)
         rslt = VAL(Man$ + "E" + Exp$)
         PRINT rslt
         IF rslt < minrslt THEN minrslt = rslt
         IF rslt > maxrslt THEN maxrslt = rslt
         totrslt = totrslt + rslt
         PRINT #2, Man$ + "E" + Exp$

WEND
PRINT "max value = "; maxrslt
PRINT "Min value = "; minrslt
PRINT "Average value = "; totrslt / count
CLOSE #1
CLOSE #2
BEEP
PRINT
INPUT "Continue? (y/n) "; ans$
```

```
IF ans$ <> "n" THEN GOTO Progloop

END
```

Appendix B: Raw Data from IR Detectors

First day of testing thin samples for 1313 nm laser

	A	Std Err	B	Std Err	C	Std Err		Std Err	
Sample	Forward	A	Back	B	Collimated	C	I_{oc}	I_{oc}	
S1	7.329E-02	8.484E-05	4.021E-01	3.236E-04	1.877E-02	1.923E-05	Use IOC		Glass, then tissue in 1st integrating sphere
S2	6.114E-02	1.348E-04	3.474E-01	8.311E-04	1.439E-01	2.372E-04	4.101E+00	1.096E-03	
S3	6.298E-02	1.505E-04	2.902E-01	4.473E-04	2.849E-02	2.814E-05	4.140E+00	8.807E-04	
S4	7.291E-02	9.628E-05	3.458E-01	1.864E-04	4.058E-02	3.271E-05	4.084E+00	2.695E-03	
S5	5.441E-02	5.447E-05	2.603E-01	8.881E-04	7.032E-02	6.319E-05	4.154E+00	2.168E-03	
S7	7.032E-02	6.319E-05	3.270E-01	5.704E-04	7.844E-02	8.877E-06	4.187E+00	1.991E-03	
S8	6.552E-02	3.299E-04	3.706E-01	3.192E-03	1.920E-02	8.922E-06	4.097E+00	1.620E-03	
IO	6.976E-01	1.323E-03	6.145E-01	file lost	3.929E+00	2.431E-03			
S1TISUE	7.579E-02	1.409E-04	4.021E-01	from S1b	1.877E-02	from S1c	3.929E+00	assume IOC	Tissue, then glass in second IS (use S1B, S1C)
NLH1	6.097E-02	2.412E-04	6.838E-02	3.706E-04				start	Laser on, no tissue holder
NOISA1	2.576E-02	3.358E-05	8.622E-02	4.435E-04		assumed:	3.929E+00	start	Laser on, tissue holder on
NOISE1	2.875E-04	9.883E-06	6.145E-01	6.749E-04	4.001E+00	2.175E-03		start x	start of test - A with laser off, B&C with laser on
NOISE1	2.875E-04	9.883E-06	4.620E-04		5.228E-05			start	Note: per lab notebook; laser off, no tissue
NOISE22	3.294E-04	1.269E-05	4.168E-04	1.474E-05	3.415E-05	1.523E-06		end	Laser off, no sample, end of testing

Note, S2-S8 were performed as per S1Tisue, S1 is different and shows little difference in putting tissue in front or back						
Note: Forgot to take IOCS1, use IOC						
Note: NOISE1 data is messed up since A is with no laser and B, C has laser- note that lab notebook has values…						
Note: Missed sample 6						
Note: Compare NOISE1 from notebook and NOISE22- very small change- insignificant relative to measured values						
Note: Compare NLH1 With NOISA1						

Second day of testing thin samples (1313 nm)

	A	Std Err	B	Std Err	C	Std Err		Std Err		
Sample	Forward	A	Back	B	Collimated	C	I_{oc}	I_{oc}		
S2	6.538E-02	2.111E-05	4.119E-01	9.175E-05	2.592E-02	1.351E-05	4.201E+00	2.058E-04		
S6	6.256E-02	3.546E-04	3.121E-01	6.107E-04			4.222E+00	6.689E-04	Disregard- Sc was not taken so this was repeated	
S6-2	7.724E-02	1.881E-05	4.230E-01	1.577E-04	4.557E-02	2.597E-06	4.365E+00	3.042E-04		
S9	6.106E-02	5.298E-05	3.302E-01	7.371E-05	3.413E-02	6.376E-05	4.352E+00	4.454E-03		
S10	7.085E-02	2.618E-05	3.746E-01	2.943E-03	1.049E-01	2.689E-05	4.374E+00	5.478E-05		
S10-2	6.011E-02	2.123E-05	3.156E-01	3.981E-05	5.917E-02	8.530E-06	4.215E+00	8.215E-04	rotated to minimize I_c	
S11	7.061E-02	1.844E-05	3.691E-01	8.272E-04	3.777E-02	8.164E-06	4.518E+00	1.195E-04	min ISC	max ISC
S12	6.812E-02	2.842E-05	3.726E-01	2.035E-04	6.417E-02	6.408E-06	4.230E+00	1.014E-04	6.300E-02	1.900E-01
S13	6.849E-02	1.746E-05	3.876E-01	4.314E-05	2.880E-02	7.123E-06	4.192E+00	1.014E-04	2.900E-02	9.600E-02
S14									Sample too small for test	
S15	6.242E-02	2.620E-05	3.173E-01	1.313E-04	4.442E-02	8.109E-06	4.201E+00	2.176E-04	4.200E-02	1.100E+00
S16	6.523E-02	2.107E-05	3.643E-01	1.944E-04	5.633E-02	7.927E-06	4.202E+00	1.629E-04	5.600E-02	1.200E-01
S17									Sample too small for test	
S18	6.746E-02	2.447E-05	3.628E-01	3.956E-05	2.819E-02	9.032E-06	4.176E+00	9.468E-05	2.700E-02	3.900E-02
S19									Sample too small for test	
S20									Sample too small for test	
S21	6.800E-02	1.938E-05	3.215E-01	1.052E-04	5.769E-02	1.573E-05	4.212E+00	1.816E-04	5.800E-02	8.800E-02
S22	6.481E-02	2.504E-05	3.399E-01	1.377E-04	4.918E-02	7.485E-06	4.200E+00	2.393E-04	4.800E-02	1.000E-01
NSH	3.691E-02	2.052E-05	4.584E-02	5.661E-05	4.203E+00	2.333E-04			Noise laser on, no tissue, no sample holder	
S22	6.481E-02	2.504E-05	3.399E-01	1.377E-04	4.918E-02	7.485E-06				
Io	5.864E-01	9.630E-04	6.698E-01	3.313E-03	4.311E+00	6.412E-03				

SH	2.190E-02	2.188E-05	6.373E-02	3.608E-05	4.215E+00	2.753E-04			Noise laser on no tissue with sample holder	
noise33	3.499E-04		4.320E-04		3.467E-05				Noise laser off, no sample holder- data from lab notebook, no file- start	
noise44	3.672E-04		4.918E-04		4.573E-05				Noise laser off, no sample holder- data from lab notebook, no file- end	
Note: Compare nsh with sh (no holder vs holder)										
Compare sh with day 1 NoiseA1										
Compare nsh with day 1 nlh1										
Note #6 repeated because of sensitivity to SC to rotation										
Compare s2_2 with values from day1 for s2										
Compare values of S_10_2 with those of S10										
Compare IO values with those of day 1 (ratios)										
Note sample #2 repeated since Sc2 from day 1 seemed too high										
Note: 10 micron samples are #12-22, others are 20 micron samples										
Compare noise33 and noise44 and day 1 Noise22										

Day 4 measurements Thick samples 1313 nm

	A	Std Err	B	Std Err	C	Std Err		Std Err		
Sample	Forward	A	Back	B	Collimated	C	I_{oc}	I_{oc}		
S23	7.086E-02	1.538E-04	2.093E-01	6.437E-04	1.273E-04	1.462E-06	4.115E+00	1.358E-03	Filter at 0.3 sec	
S23-2	7.467E-02	8.710E-05	2.245E-01	3.761E-05	1.157E-04	7.685E-07	4.039E+00	8.391E-04	Filter at 1 sec	
S23-W	1.480E-01	5.972E-04	1.111E-01	8.749E-05	1.280E-04	8.998E-07	3.903E+00	7.198E-04	put white side forward	
S23-W2	8.562E-02	9.655E-05	2.365E-01	1.690E-04	1.177E-04	6.581E-07	3.862E+00	2.714E-04	Sample on 1st int sphere?	
S24	8.127E-02	1.789E-04	1.911E-01	2.939E-04	1.522E-04	1.777E-06	4.006E+00	5.264E-04	Filter at 0.3 sec	
S24-2	8.576E-02		2.507E-01	4.711E-04	2.275E-04	1.662E-06	4.185E+00	6.403E-03	Filter at 1 sec. S24-2A data file missing, used lab notebook data	
S25	7.796E-02	7.291E-05	1.614E-01	1.278E-04	9.001E-05	7.556E-07	4.004E+00	3.275E-03	2nd int sphere	
S26	7.912E-02	6.679E-05	2.183E-01	1.421E-04	1.464E-04	9.031E-07	4.241E+00	8.781E-03	2nd int sphere	
S27	8.710E-02	2.124E-04	2.552E-01	1.184E-04	1.885E-04	7.659E-07	4.112E+00	7.065E-03	2nd int sphere	
S28	8.497E-02	2.240E-04	2.468E-01	5.393E-04	1.856E-04	8.988E-07	4.001E+00	2.445E-03	2nd int sphere	
S29	1.122E-01	1.670E-05	2.200E-01	2.744E-05	9.778E-05	6.571E-07	3.839E+00	2.312E-04	2nd int sphere	
S29-1	2.095E-01	2.759E-05	1.283E-01	2.224E-04	9.798E-05	6.515E-07	3.853E+00	1.755E-04	1st int sphere	
S30	1.279E-01	6.028E-05	1.898E-01	2.677E-05	9.467E-05	1.132E-06	3.844E+00	6.121E-05	2nd int sphere or 1st?	
S31	9.814E-02	1.230E-05	2.428E-01	3.055E-05	1.146E-04	6.672E-07	3.858E+00	1.528E-04	2nd int sphere	
S32	1.033E-01	1.376E-05	1.950E-01	1.718E-05	9.312E-05	7.458E-07	3.863E+00	6.152E-05	2nd int sphere	
S33	9.933E-02	1.432E-05	2.329E-01	1.816E-05	1.198E-04	7.443E-07	3.850E+00	1.979E-04	2nd int sphere	
S34	8.541E-02	1.691E-05	2.844E-01	2.557E-05	1.874E-04	8.772E-07	3.832E+00	6.644E-05	6th int sphere	
Noise 33	3.365E-04	1.147E-05	4.816E-04	1.719E-05	3.534E-05	1.468E-06			Noise laser off start	
Noise 44	1.302E-04	5.095E-06	3.059E-04	1.133E-05	1.668E-05	6.603E-07			Noise laser off end	
SH	2.190E-02	2.188E-05	6.373E-02	3.608E-05	4.215E+00	2.753E-04			Day 2 data Noise laser on no tissue with sample holder	
Io	5.864E-01	9.630E-04	6.698E-01	3.313E-03	4.311E+00	6.412E-03			9/11 data for Io	
Noise	2.093E-04	8.896E-06	2.964E-04	8.914E-06	1.276E-05	4.797E-07	1.584E-05	6.141E-07	last two are a repeat of C	

Note compare noise33 and 44, along with past noise values											
Note: 23 and 24 were done with filter at 0.3 sec, while 23-2 and 24-2 with filter at 1 sec											
Note dark skin forward- samples 23-27 are dark											
Note, did not take data with laser for noise- use day-2 data											
Note, did not take data for Io- use day-2 data											
Note calculate C sensor vs noise…											
Note: compare s23 and s23-2, as well as s24, s24-2, same sample, two filter settings											

Day-5 testing (1064 nm) thin tissue

	A	Std Err	B	Std Err	C	Std Err		Std Err		Std Err	
Sample	Forward	A	Back	B	Collimated	C	I_{oc}	I_{oc}	C_{rot}	C_{rot}	
S1	2.303E-02	1.912E-05	1.561E-01	3.026E-05	1.969E-02	5.391E-06	4.100E+00	I0C-4	9.085E-03	9.272E-05	Use I_{oc} from IOC-4, since data missing
S2	2.196E-02	1.995E-05	1.490E-01	2.603E-05	3.207E-02	3.499E-06	4.094E+00	1.271E-04	9.594E-02	5.984E-03	
S3	1.269E-02	1.737E-05	1.032E-01	2.863E-05	2.703E-02	7.640E-06	4.099E+00	7.147E-05	3.144E-02	3.199E-04	
S4	2.149E-02	1.369E-05	1.500E-01	3.178E-05	1.402E-02	1.320E-06	4.122E+00	5.801E-05	2.045E-02	5.862E-04	
S5	1.976E-02	1.816E-05	9.732E-02	2.532E-05	2.744E-02	3.843E-06	4.127E+00	5.995E-05	2.885E-02	1.976E-04	
S6	2.203E-02	1.739E-05	1.265E-01	2.672E-05	4.388E-02	4.546E-06	4.137E+00	9.684E-05	1.461E-01	1.058E-02	
S7	2.047E-02	1.908E-05	1.186E-01	2.429E-05	2.177E-02	2.740E-06	4.108E+00	2.298E-04	2.539E-02	4.247E-04	
S8	2.328E-02	2.065E-05	1.506E-01	2.849E-05	8.727E-03	1.951E-06	4.105E+00	5.881E-05	9.168E-03	1.000E-04	
S9	2.040E-02	1.461E-05	1.125E-01	3.180E-05	3.185E-02	7.679E-06	4.104E+00	6.276E-05	2.463E-02	4.421E-04	
S10	2.231E-02	1.766E-05	1.347E-01	2.652E-05	1.101E-01	7.490E-06	4.121E+00	1.339E-04	9.616E-02	2.334E-03	
S11	2.238E-02	1.719E-05	1.382E-01	2.606E-05	3.366E-02	8.233E-06	4.117E+00	5.801E-05	3.150E-02	1.703E-03	
S12	2.280E-02	1.613E-05	1.337E-01	2.482E-05	5.252E-02	3.302E-06	4.117E+00	1.149E-04	5.584E-02	3.716E-03	
S13	2.195E-02	1.754E-05	1.322E-01	2.338E-05	4.903E-02	1.753E-06	4.116E+00	5.356E-05	3.767E-02	8.952E-04	
S15	2.034E-02	2.879E-05	1.310E-01	4.443E-05	4.796E-02	1.707E-05	4.118E+00	1.406E-04	3.606E-02	7.241E-04	Slight error in file labeling IOC
S16	2.169E-02	2.460E-05	1.547E-01	2.975E-05	4.637E-02	3.643E-06	4.120E+00	7.135E-05	6.417E-02	1.837E-03	
S17											
S18	2.237E-02	1.527E-05	1.346E-01	3.530E-05	1.625E-02	2.206E-06	4.123E+00	1.101E-04	1.663E-02	2.029E-04	
S21	2.200E-02	1.725E-05	1.081E-01	2.280E-05	3.377E-02	2.666E-06	4.112E+00	3.998E-05	3.487E-02	2.931E-04	
S22	2.168E-02	2.073E-05	1.067E-01	2.595E-05	6.064E-02	5.964E-06	4.122E+00	8.559E-05	4.386E-02	1.263E-03	
Noise 66	3.352E-04	1.101E-05	4.687E-04	1.710E-05	4.211E-05	2.068E-06					Noise at start
Noise	3.103E-04	1.303E-05	5.257E-04	1.839E-05	2.674E-05	8.932E-07					Noise at end

77											
NSH	1.492E-03	2.091E-05	1.915E-03	2.242E-05	4.136E+00	1.732E-04					Noise, laser on, no tissue holder in place
SH2	9.407E-04	2.218E-05	2.265E-03	2.355E-05			4.072E+00	use same as closest (I1s)			Noise, laser on, tissue holder on
SH3	8.876E-04	1.788E-05	2.325E-03	2.124E-05			4.122E+00	use closest I0C1s22			End noise laser on tissue holder on
I1S	1.974E-02	1.985E-05	1.557E-01	3.353E-05	2.508E-02	4.123E-06	4.072E+00	5.308E-05			Tissue on 1st integrating sphere
IO-3	3.132E-01	2.086E-05	3.106E-01	4.992E-05	4.077E+00	2.573E-04					IO's with no tissue holder
IO-4			3.204E-01	4.727E-05	4.100E+00	7.790E-05					IO's with tissue holder
IC ROT S6	2.151E-02	4.343E-05	1.284E-01	2.311E-04					1.461E-01	1.058E-02	
Avg SH	2.232E-04		5.602E-04								Average os SH2 and SH3 /IOC's
Note: compare IO3 with IO4											
Compare noise 66 and noise77 along with all other noise values											
Compare I1s with S1 (1st vs 2nd integrating sphere)											
IoC from S1 missing											

Compare IC Rot S6 with S6 (in former A&B are also rotated) plot the rotated ones									
compare sh2 start and sh3 end									

Day-6 testing thick samples (1064 nm)

	A	Std Err	B	Std Err	C	Std Err		Std Err		Std Err	
Sample	Forward	A	Back	B	Collimated	C	I_{oc}	I_{oc}	C_{rot}	C_{rot}	
S23	3.802E-02	2.182E-05	1.291E-01	5.720E-05	7.970E-05	1.476E-06	4.106E+00	6.045E-04	**8.351E-05**	**from lab notebook**	
S24	3.939E-02	2.152E-05	1.248E-01	2.338E-05	9.191E-05	1.701E-06	4.105E+00	8.363E-04	1.016E-04	3.113E-06	
S25	3.487E-02	1.783E-05	1.296E-01	2.786E-05	8.847E-05	1.472E-06	4.121E+00	2.901E-04	8.360E-05	1.594E-06	
S26	3.575E-02	1.980E-05	1.252E-01	2.998E-05	8.243E-05	1.537E-06	4.129E+00	9.186E-05	9.292E-05	1.474E-06	
S27	3.054E-02	1.608E-05	1.519E-01	3.662E-05	1.447E-04	2.601E-06	4.128E+00	4.660E-04	1.351E-04	2.005E-06	Note, I_{oc} was fixed using raw data
S28	2.931E-02	2.013E-05	1.556E-01	2.510E-05	1.394E-04	1.956E-06	4.139E+00	1.065E-04	1.485E-04	1.912E-06	
S29	3.238E-02	2.441E-05	1.768E-01	2.639E-05	2.117E-04	3.024E-06	4.123E+00	1.229E-04	2.398E-04	3.573E-06	
S30	1.961E-02	1.737E-05	2.163E-01	6.639E-05	7.555E-04	2.246E-06	4.103E+00	5.688E-05	6.486E-04	1.488E-05	
S31	2.831E-02	1.946E-05	1.930E-01	2.702E-05	2.983E-04	2.548E-06	4.139E+00	9.241E-05	4.573E-04	1.408E-05	
1S132	2.676E-02	1.920E-05	1.999E-01	2.737E-05	2.806E-04	2.616E-06	4.139E+00	6.970E-05	2.508E-04	3.511E-06	Repeat of 32
S323	2.300E-02	1.471E-05	2.079E-01	2.854E-05	3.996E-04	1.922E-06	4.140E+00	6.029E-05	4.418E-04	4.874E-06	
S32	3.253E-02	1.825E-05			2.019E-04	1.448E-06					Eliminate due to error in collecting data
S33	2.058E-02	1.628E-05	1.963E-01	2.817E-05	5.035E-04	1.949E-06	4.125E+00	5.466E-05	5.519E-04	5.156E-06	
S34	1.948E-02	1.878E-05	2.249E-01	2.012E-05	1.514E-03	3.122E-06	4.126E+00	7.507E-05	1.845E-03	1.991E-05	
Noise 88	3.767E-04	1.042E-05	4.770E-04	1.725E-05	2.501E-05	7.754E-07					Noise start
Noise 99	3.136E-04	1.216E-05	4.864E-04	1.339E-05	3.286E-05	1.169E-06					Noise end
SH	9.048E-04	1.667E-05	2.364E-03	2.395E-05			4.139E+00	copied from 1s132			Noise laser on tissue holder on
IO	3.132E-01		3.106E-01		4.077E+00		used IO-3 from Day-5 testing				

Note compare noise88 with noise99 with other no laser noise											
Note Crot for S23 was not recorded on a computer file											
Ioc for s27 was reconstructed from file. Data was collected with tissue in place for part of the time											
For SH use IO closest which is ioc1s323											
Note used IO-3 from Day-5 testing											

Day 8 testing (1313 and 1064 nm laser) – selected samples

	A	Std Err	B	Std Err	C	Std Err		Std Err		Std Err	
Sample	Forward	A	Back	B	Collimated	C	I_{oc}	I_{oc}	C_{rot}	C_{rot}	
S1	2.266E-02	1.804E-05	1.429E-01	2.940E-05	1.188E-02	2.240E-06	3.959E+00	2.200E-04	1.377E-02	4.315E-04	12S1_
S8	2.233E-02	1.862E-05	1.444E-01	3.624E-05	9.935E-03	1.968E-06	3.955E+00	1.597E-04	9.824E-03	1.097E-04	12S8_
S10	2.102E-02	1.668E-05	1.312E-01	2.511E-05	9.843E-02	2.827E-05	3.966E+00	1.257E-04	8.776E-02	3.933E-03	12S10_
S16	2.058E-02	1.680E-05	1.458E-01	3.211E-05	1.257E-01	1.362E-05	3.977E+00	1.724E-04	9.949E-02	6.412E-03	12S16_
S18	2.149E-02	1.608E-05	1.352E-01	2.744E-05	1.467E-02	2.472E-06	3.942E+00	7.441E-05	1.475E-02	2.360E-04	12S18_
S21	2.148E-02	2.032E-05	1.113E-01	2.872E-05	3.577E-02	1.410E-06	3.956E+00	3.539E-04	3.672E-02	4.327E-04	12S21_
S22	2.124E-02	1.900E-05	1.102E-01	2.454E-05	3.043E-02	3.013E-06	3.971E+00	6.994E-05	2.892E-02	6.092E-04	12S22_
SW	1.044E-02	1.615E-05	2.425E-03	2.308E-05	3.799E+00	1.094E-04	3.969E+00	1.251E-04			1sw1_ Water 1mm
SX	2.236E-02	1.282E-05	1.500E-01	2.916E-05	8.669E-03	1.515E-06	3.957E+00	7.973E-05	9.371E-03	7.144E-05	Old tissue sample 20 micron 1SX
SY	2.204E-02	1.621E-05	1.515E-01	3.327E-05	1.801E-02	2.216E-06	3.931E+00	1.082E-04	1.606E-02	7.577E-04	Old tissue sample 20 micron 1SY
SH5	1.277E-03	2.024E-05	1.756E-03	2.933E-05	3.959E+00	from S1 I_{oc}					Noise laser on sample holder on- use Io from I0C1SY
SH-6	8.208E-04	1.394E-05	2.150E-03	1.991E-05	3.931E+00	from I0C1SY					Noise laser on sample holder on- use Io from S2
IO-3	3.132E-01	2.086E-05	3.106E-01	4.992E-05	4.077E+00	2.573E-04	Use Io from 9/14 data				

1.3 micron laser

	A	Std Err	B	Std Err	C	Std Err		Std Err		
Sample	Forward	A	Back	B	Collimated	C	I_{oc}	I_{oc}	C_{rot}	
NSH7	2.586E-02	1.687E-05	3.778E-02	2.724E-05	4.199E+00	6.113E-04				
SH7	1.554E-02	1.422E-05	4.361E-02	4.482E-05	4.179E+00	3.302E-04				
S1-1	5.873E-02	1.898E-05	3.520E-01	3.987E-05	1.946E-02	2.892E-06	3.907E+00	3.390E-04	2.149E-02	4.289E-04
S8-1	5.730E-02	5.926E-05	3.274E-01	1.110E-04	6.720E-02	2.291E-04	4.223E+00	1.125E-02	2.687E-02	1.206E-03
S10-1	5.533E-02	2.907E-05	3.008E-01	1.544E-04	8.774E-02	6.546E-05	4.203E+00	3.225E-03	1.552E-01	1.139E-02
S16-1	5.483E-02	1.888E-05	3.483E-01	9.133E-05	4.089E-02	2.920E-05	4.295E+00	1.238E-03	7.684E-01	1.018E-01
S18-1	5.804E-02	4.696E-05	3.290E-01	4.273E-05	3.094E-02	7.773E-06	4.149E+00	9.901E-04	3.055E-02	2.170E-04
S21-1	5.717E-02	1.662E-05	3.515E-01	3.823E-05	6.692E-02	8.959E-06	4.130E+00	2.686E-04	1.545E-01	2.395E-02
S22-1	5.648E-02	1.623E-05	3.883E-01	7.734E-05	1.295E-01	7.570E-05	4.018E+00	3.715E-04	3.372E-01	3.580E-02
SX-1	5.951E-02	2.163E-05	3.489E-01	3.083E-05	2.384E-02	1.827E-06	3.864E+00	6.414E-04	2.511E-02	4.241E-04
SY-1	5.300E-02	2.157E-05	2.988E-01	5.035E-05	9.026E-01	4.215E-04	4.232E+00	1.045E-04	6.679E-01	6.296E-02
SW-1	3.942E-02	1.967E-05	2.691E-02	3.073E-05	3.752E+00	8.118E-04	4.220E+00	5.624E-04		

Repeat with tissue in 1st integrating sphere
1.3 micron laser

	A	Std Err	B	Std Err	C	Std Err		Std Err			
Sample	Forward	A	Back	B	Collimated	C	I_{oc}	I_{oc}	C_{rot}		
SW-2	1.241E-01	2.889E-05	6.817E-02	2.156E-05	9.780E-02	7.662E-06	4.160E+00	1.025E-04	3.902E-01	5.394E-02	2SW_2
S21-2	9.917E-02	2.164E-05	1.928E-01	2.852E-05	1.749E-02	3.595E-06	4.135E+00	7.406E-05	5.264E-02	6.722E-03	2S21_2
S10-2	1.245E-01	1.983E-05	1.729E-01	3.107E-05	3.499E-02	2.494E-06	4.153E+00	3.994E-04	4.121E-01	6.126E-02	2S10_2
S10-2-R	1.063E-01	1.998E-03	1.855E-01	2.336E-03	3.499E-02	copy Ic	4.153E+00	copy I_{oc}	4.121E-01	copy I_{rot}	2I_R10 is rotation of A and B, use same ICROT
NSH8	2.135E-02	1.705E-05	3.050E-02	1.853E-05	4.172E+00	4.658E-04					noise laser off
SH8	1.469E-02	1.652E-05	3.392E-02	3.220E-05	4.147E+00	2.642E-04		end laser on tissue holder on 2nd integrating sphere (normal)			end laser on tissue holder on
SH9	6.674E-02	2.094E-05	3.334E-02	3.147E-05	2.252E+00	1.699E-04		* interference on Ioc- ignore			end laser on tissue holder 1st integrating sphere

SH10	2.514E-02	1.773E-05	3.623E-02	2.706E-05	4.169E+00	4.937E-04		end laser on tissue holder on 1st integrating sphere (abnormal)			repeat os SH9
Noise 10	3.018E-04	1.044E-05	4.406E-04	1.630E-05	2.738E-05	9.816E-07					Noise at start all off
Noise 12	3.225E-04	1.338E-05	4.670E-04	1.709E-05	2.812E-05	8.811E-07					end no sample holder, no laser
WSH	5.803E-02	3.689E-05	6.889E-02	3.081E-05	3.589E+00	1.754E-04	4.184E+00	2.850E-04			water, holder on 2nd integrating sphere
IO	6.860E-01	4.550E-05	6.984E-01	8.747E-05	4.271E+00	2.127E-04					no tissue holder
Note: compare Noise 10 with Noise 12, and all past noise											
sha5 uses I_{oc} from S1 (closest sample)											
Compare sh5 and sh6											
sh6 uses IoC1Sy as closest Io											